

REVIEW

[View Article Online](#)
[View Journal](#) | [View Issue](#)



Cite this: *Chem. Sci.*, 2021, **12**, 14987

Computational and data driven molecular material design assisted by low scaling quantum mechanics calculations and machine learning†

Wei Li, *^a Haibo Ma, *^{ab} Shuhua Li ^a and Jing Ma *^{ab}

Electronic structure methods based on quantum mechanics (QM) are widely employed in the computational predictions of the molecular properties and optoelectronic properties of molecular materials. The computational costs of these QM methods, ranging from density functional theory (DFT) or time-dependent DFT (TDDFT) to wave-function theory (WFT), usually increase sharply with the system size, causing the curse of dimensionality and hindering the QM calculations for large sized systems such as long polymer oligomers and complex molecular aggregates. In such cases, in recent years low scaling QM methods and machine learning (ML) techniques have been adopted to reduce the computational costs and thus assist computational and data driven molecular material design. In this review, we illustrated low scaling ground-state and excited-state QM approaches and their applications to long oligomers, self-assembled supramolecular complexes, stimuli-responsive materials, mechanically interlocked molecules, and excited state processes in molecular aggregates. Variable electrostatic parameters were also introduced in the modified force fields with the polarization model. On the basis of QM computational or experimental datasets, several ML algorithms, including explainable models, deep learning, and on-line learning methods, have been employed to predict the molecular energies, forces, electronic structure properties, and optical or electrical properties of materials. It can be conceived that low scaling algorithms with periodic boundary conditions are expected to be further applicable to functional materials, perhaps in combination with machine learning to fast predict the lattice energy, crystal structures, and spectroscopic properties of periodic functional materials.

Received 10th May 2021
Accepted 12th October 2021

DOI: 10.1039/d1sc02574k
rsc.li/chemical-science

^aKey Laboratory of Mesoscopic Chemistry of Ministry of Education, Institute of Theoretical and Computational Chemistry, School of Chemistry and Chemical Engineering, Nanjing University, Nanjing 210023, China. E-mail: majing@nju.edu.cn; wli@nju.edu.cn; haibo@nju.edu.cn

^bJiangsu Key Laboratory of Advanced Organic Materials, Jiangsu Key Laboratory of Vehicle Emissions Control, Nanjing University, Nanjing 210023, China



Wei Li received his Ph.D degree in theoretical chemistry from Nanjing University (2007) and then worked at Michigan State University as a postdoctoral associate. He is currently an associate professor of chemistry at Nanjing University (since 2011). He has received the Tang Au-Qing youth award in theoretical chemistry from the Chinese Chemical Society (2014). His research focuses on the development of low or linear scaling electronic structure methods and their applications to biological systems, molecular materials, and solutions.

† Electronic supplementary information (ESI) available: Selected studies of using low-scaling quantum mechanics methods or machine learning to study molecular materials. See DOI: [10.1039/d1sc02574k](https://doi.org/10.1039/d1sc02574k)



Haibo Ma is a Professor of Theoretical Chemistry at Nanjing University. He received a B.S. and a Ph.D. from Nanjing University in 2002 and 2007 respectively. He has received the Humboldt research Fellowship from the Alexander von Humboldt foundation (2007–2009) and the Tang Au-Qing youth award in theoretical chemistry from the Chinese Chemical Society (2018). His main research interests focus on the development of new quantum chemical methods for strongly correlated systems and theoretical investigation of excited state processes in optoelectronic materials.



1 Introduction

High-throughput computations have played important roles in material design in recent years.^{1–3} The prediction of the structures and properties of newly designed materials is useful to guide molecular syntheses and device fabrication.^{4–6} For example, theoretical computations have been employed to assist designing layered and inorganic crystals,⁷ two-dimensional materials,³ energy-related materials,^{5,8} functional organic materials,^{6,9} and polymeric materials.¹⁰ Both quantum mechanics (QM) and classical molecular mechanics (MM) based molecular simulations are widely employed to compute the material with oligomer/cluster models or periodic boundary conditions (PBCs). PBC calculations are widely applied to atomic and molecular crystals and covalent-bonded three- or two-dimensional inorganic materials.^{3,7} For many molecular materials (e.g., organic materials with large π -conjugation cores or polymeric materials),^{6,9,10} QM calculations with a PBC model are still very expensive, due to their large sized cell boxes, and only PBC MM calculations are affordable for high throughput calculations. However, in order to compute the electronic structure properties (such as optical, electrical, or magnetic properties) of materials, to obtain a more accurate material structure or to benchmark the empirical intermolecular potentials, density functional theory (DFT) or even more accurate *ab initio* electron correlation methods using a cluster model (or a PBC model for molecular materials with small molecules) are required.^{11,12}

DFT scales as $O(N^{3–4})$ with the number of electrons, N , increased and is expensive for large-sized complex material systems.¹³ To accelerate the design of new materials, a high-throughput screening scheme by integrating multi-scale calculations is employed in computational materials, in which the expensive QM calculations are the bottleneck in the whole



Shuhua Li received his Ph.D. in physical chemistry from Nanjing University in 1996 and then worked at Nanjing University and Texas A&M University as a postdoctoral researcher. Then he began to work at Nanjing University as an associate professor (2000–2002) and professor of chemistry (since 2002). He has received the Pople Medal of Asian Pacific Association of Theoretical and Computational Chemists (2008) and the First Prize of Natural Science Award from the Chinese Ministry of Education (2019). In 2017, he was elected as a member of the International Academy of Quantum Molecular Science. His research interests focus on the development of novel multi-reference and linear scaling electronic structure algorithms and the computational design of new chemical reactions.

computational processes. Conventional QM methods are not available for molecular material systems with thousands of atoms. Higher-level wave function-based electron correlation calculations are even more expensive. The development and implementation of low or even linear scaling QM methods are hence very urgent for material design. The realization of low-scaling DFT or electron correlation calculations is one of the core challenges in the quantum chemistry community in the last two decades. Due to the difficulty in the theoretical treatment of the ground state and excited states of π -electron delocalized and metal-containing systems, application examples of low or linear scaling methods to materials are far fewer than the computations of water clusters and proteins, as shown in Table S1.[†] Several low-scaling strategies, such as density matrix-based, local correlation, and fragment-based methods, were used to predict the ground-state energies, structures, and molecular properties of large systems. For example, a local correlation cluster-in-molecule (CIM) method was used to predict the binding energies in aqueous zinc-organic batteries;¹⁴ a divide-and-conquer method was developed to optimize the molecular geometries of conjugated oligomers;¹⁵ density-functional perturbation theory (DFPT) was employed to compute the polarizabilities of large organic molecules;¹⁶ a generalized energy-based fragmentation (GEBF) method was used to predict the infrared (IR) and nuclear magnetic resonance (NMR) spectra of large supramolecular coordination complexes.¹⁷

For characterizing the electronic structure features in photophysics and photochemistry, fragment-based methods have been successfully applied in accurately calculating excited states in large systems and condensed phases at a high QM level, ranging from simulating optical spectra of aggregation-induced emission (AIE) in molecular crystal materials¹⁸ to elucidating excitonic interactions in the Fenna–Matthews–



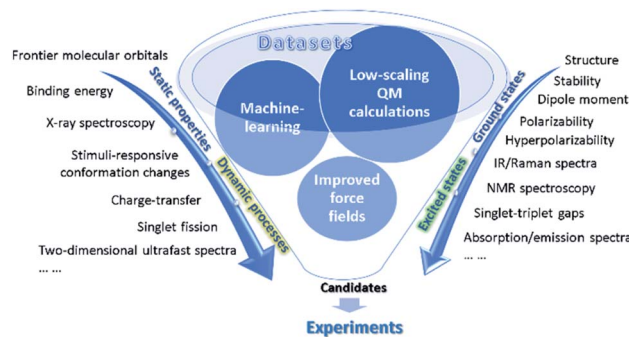
Jing Ma received her PhD (1998) degree in Theoretical Chemistry from Nanjing University, China. She was a JSPS fellow (1998–2000) at Gifu University, Japan. After that she began to work at Nanjing University as an associate professor (2000–2005) and professor of chemistry (since 2005). She has received several awards, including the Outstanding Young Chemist Award of Chinese Chemical Society and Chinese Young Women Scientists Awards. Her research is concentrated on electrostatic polarization in low-scaling QM calculations and force field simulations of oligomers and stimuli-responsive materials with unique optical and electrical properties. Recently she also showed interest in material datasets and data-driven material design.



Olson complex (6853 atoms).¹⁹ In addition, *ab initio* exciton models can be used for the low-cost study of various excited state processes in complex environments, *e.g.*, optical generation of long-range charge-transfer states in electron donor/acceptor heterojunctions²⁰ and singlet fission in crystalline tetracene.²¹ Moreover, novel low-scaling quantum dynamics methods like time-dependent density matrix renormalization group (tDMRG)²² and multi-configuration time-dependent Hartree (MCTDH)²³ were recently employed for the accurate simulation of real-time nonadiabatic dynamics^{24,25} and ultrafast one- or two-dimensional electronic spectroscopy with vibrational resolution^{26,27} in complicated systems with a large number of nuclear and electron degrees of freedom, helping build a bridge between theory and experiment in photophysics and photochemistry.

Driven by the fast development of computer science and artificial intelligence, as well as the availability of massive data, efficient data-mining techniques, especially machine learning (ML) approaches, have been widely used in materials science.^{28–32} The amount of ML-related literature is growing explosively. It is impossible to give a complete list of all those publications, and in Table S2,† we collect some representative applications of ML models in materials. For instance, combining experiments with microscopic structural descriptors and/or computational simulations, quantitative structure–property relationship (QSPR) models can be derived for predicting a variety of properties of materials.^{33,34} Furthermore, such predictive models can be combined with virtual screening by high throughput computations to accelerate the discovery and development of new functional materials with favourable properties and provide insight into the factors governing these properties.^{35,36} On the other hand, ML techniques enabled numerous advances for simulating materials previously out of reach due to the computational complexity of traditional electronic-structure methods. Those exciting advances include constructing ML-based force fields (FFs),³⁷ speeding up excited state calculations,³⁸ predicting spectroscopy properties,³⁹ and computer-aided synthesis planning.⁴⁰

In this review, we will emphasize on computational and data driven molecular material design assisted by low scaling QM calculations and machine learning based on examples from the authors as well as other groups (see Fig. 1). We begin by introducing low scaling ground-state quantum mechanics for the computations of molecular materials, including polymer oligomers, supramolecular complexes, and electrode materials. Then, to treat the excited states in optoelectronic materials, we present low scaling excited-state QM and quantum dynamics (QD) methods and use them to describe microscopic photo-physical mechanisms in organic semiconductors. In combination with the low-scaling QM calculations, the improved force fields with the polarizable partial charges or fragment dipole moments are applicable to the simulations of dynamic conformational changes in stimuli-responsive monolayers⁴¹ or [2]-rotaxane.⁴² Furthermore, we introduce the applications of explainable models and deep learning methods to the designs of organic solar cells⁴³ and predictions of molecular or material properties. The efficiency of building the force fields from the



Rational design of molecular materials

Fig. 1 Schematic illustration of the increasingly important role played by the low-scaling QM calculations, the improved force fields and machine learning methods in the prediction of material properties from ground states to excited states and from static properties to dynamic processes.

low scaling QM-based on-line machine learning force field is also discussed.^{44,218} Finally, the perspective discusses some directions for further improvement and proposes future lines of this exciting and quickly developing field.

2 Low scaling QM methods for large-sized molecules and aggregates

2.1 Low scaling calculations of ground-state energies and properties

The understanding of ground-state molecular structures, non-covalent interactions or binding energies, and various molecular properties is crucial in the rational design of molecular materials, including oligomers, monolayers on surfaces, molecular crystals, *etc.* Due to the large size of molecular materials (*e.g.*, polymers and molecular aggregates), empirical force fields are usually employed in their simulations. However, the force field parameters are not always transferable for all the studied materials, especially for charged and π -conjugated polymers. Quantum mechanics calculations are hence required to predict molecular structures and to describe intermolecular interactions without the pre-determination of empirical parameters. DFT is widely used in computational material fields due to the balance between computational cost and accuracy. The lack of long-range attractive terms for describing non-bonded interactions is one of the limitations of some DFT functionals in describing the noncovalent intermolecular interactions in molecular aggregates and super-molecular assembly. To overcome the difficulties and to improve the performance of DFT methods, some functionals, such as B97D3⁴⁵ and ω B97XD,⁴⁶ were developed to take noncovalent interactions into account. Furthermore, more accurate interaction energies could be obtained by *ab initio* electron correlation methods, such as second-order Møller–Plesset perturbation theory (MP2) and coupled cluster (CC) theory. However, the conventional electron correlation methods are very expensive for large sized systems due to their high



computational scaling with the number of basis functions, N_b , or electrons. For example, the scalings of MP2 and CC singles and doubles (CCSD) methods are $O(N_b^5)$ and $O(N_b^6)$, respectively. The gold standard CCSD with perturbative triples corrections [CCSD(T)] method even scales as $O(N_b^7)$. To alleviate such high computation scales, low (or even linear) scaling quantum chemistry methods were developed for the fast ground-state calculations of large systems.^{47–49}

In general, there exist two categories of linear or low scaling algorithms, including “first-principles” methods and fragmentation methods. The “first-principles” methods are further classified in two groups, *i.e.*, linear Hartree–Fock (HF) and DFT algorithms and local correlation methods. In the first-principles based linear or low scaling HF and DFT methods, efficient algorithms are employed to compute integrals or matrix elements. For example, integral screening,⁵⁰ fast multipole method (FMM),⁴⁷ order- N exchange method,⁵¹ and LinXC scheme⁵² are employed to compute two-electron integrals, Coulomb matrices, exchange matrices, and exchange–correlation density functional quadrature, respectively. The density matrix search (DMS) approach⁵³ is used to avoid the diagonalization of the Fock matrix. In the local correlation method, the electron correlation equations are approximately solved in the representations of the localized molecular orbital (LMO) or atomic orbital (AO) by neglecting the correlation between spatially distant orbitals. The local correlation method (Fig. 2) was first proposed by Pulay *et al.* at the MP2 level,⁵⁴ and generalized by Werner *et al.* at the CCSD level.⁵⁵ In the last two decades, the local correlation methods were further developed by various groups.^{48,56–60} For example, in the CIM approach^{60–62} developed by us, the correlation energy contributions of occupied LMOs can be approximately obtained from various clusters, each of which consists of only a subset of occupied LMOs and corresponding unoccupied orbitals and atomic basis. In summary, chemical intuition is not involved in the “first-principles” methods and the corresponding program could be a black-box for users. Recently, analytic energy gradients were implemented in the CIM approach, which enables the geometry optimization of large systems with up to 174 atoms.⁶³ The dataset of CIM-MP2 or CIM-CCSD binding energies of supermolecules and molecular aggregates was also reported,⁶⁴ providing the benchmark data for DFT functional and force-field validations. However, high-order analytical energy

derivatives with respect to nuclear coordinates or external electronic (or magnetic) fields are still hard to obtain for the local correlation methods because of requirements of some special integrals.

On the other hand, fragmentation methods provide a more efficient way to compute the energy or electronic structure properties of large sized systems. In this category, density-matrix based fragmentation and energy-based fragmentation approaches were developed. The density-matrix based fragmentation approach was first proposed by Yang and co-workers in the divide-and-conquer (DC) method at the DFT level,⁶⁵ which was significantly extended by Nakai and co-workers to various *ab initio* electron correlation levels.^{66,67} Within the framework of the density-matrix based approaches, the total density matrix of a target system is obtained from the density matrices or molecular orbitals (MOs) of subsystems. Then, the total ground energy or molecular properties of the total system are computed from the approximate total density matrix. Various density matrix based approaches were also developed, such as the adjustable density matrix assembler (ADMA) method,⁶⁸ the elongation method,⁶⁹ and the molecular fractionation with conjugated caps (MFCC) approach.⁷⁰ The LMO assembler (LMOA) method⁷¹ has been proposed with the total density matrix being assembled by the LMOs of the central region of subsystems or electrostatically embedded subsystems.⁷² However, the density-matrix based methods for large systems require high computational costs of integrals and large resources (memory or disk) for the entire system.

In comparison with density-matrix based approaches, energy-based fragmentation approaches (Fig. 2) need less computational cost and fewer resource requirements for the total system, because in such methods the total ground-state energy (or energy derivatives) of a target system is directly represented as the combination of the corresponding energies (or energy derivatives) of various subsystems.⁷³ Those subsystems could be calculated at both DFT and post-Hartree–Fock levels with existing quantum chemistry packages. In addition, the calculations of subsystems could be coarse-grain paralleled and distributed in different computer nodes, and each subsystem could be fine-grain paralleled with processors within a node. The theoretical framework of molecular fragments was employed to develop QM-based force fields for the simulations of liquids and solutions in the effective fragment potential⁷⁴ method and explicit polarization⁷⁵ method, respectively. Based on many-body expansion, Kitaura and co-worker proposed the fragment molecular orbital (FMO) method,⁷⁶ in which orbitals are employed to saturate the dangling bonds. Energy-based fragmentation methods for the ground-state calculations of large sized molecules are independently proposed by three groups^{77–79} in 2005. To take long-range electrostatic interactions into account for long oligomer systems with the charged group, we developed an electrostatically embedding scheme by placing point charges at the charge centres in each subsystem calculation.⁸⁰ Furthermore, by introducing background point charges on those atoms outside the subsystems, we further proposed the GEBF approach.⁸¹ Thus, in our GEBF approach, the ground-state energies (or energy derivatives) of a target molecule could

Linear Scaling Methods for Large Systems

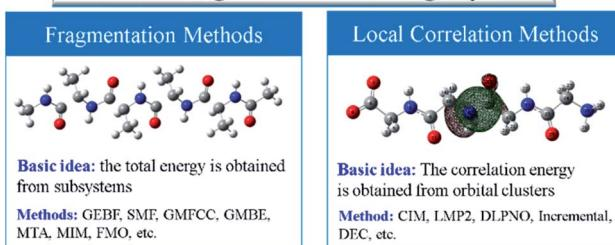


Fig. 2 Two kinds of linear scaling methods for large sized systems: local correlation methods and fragmentation methods.



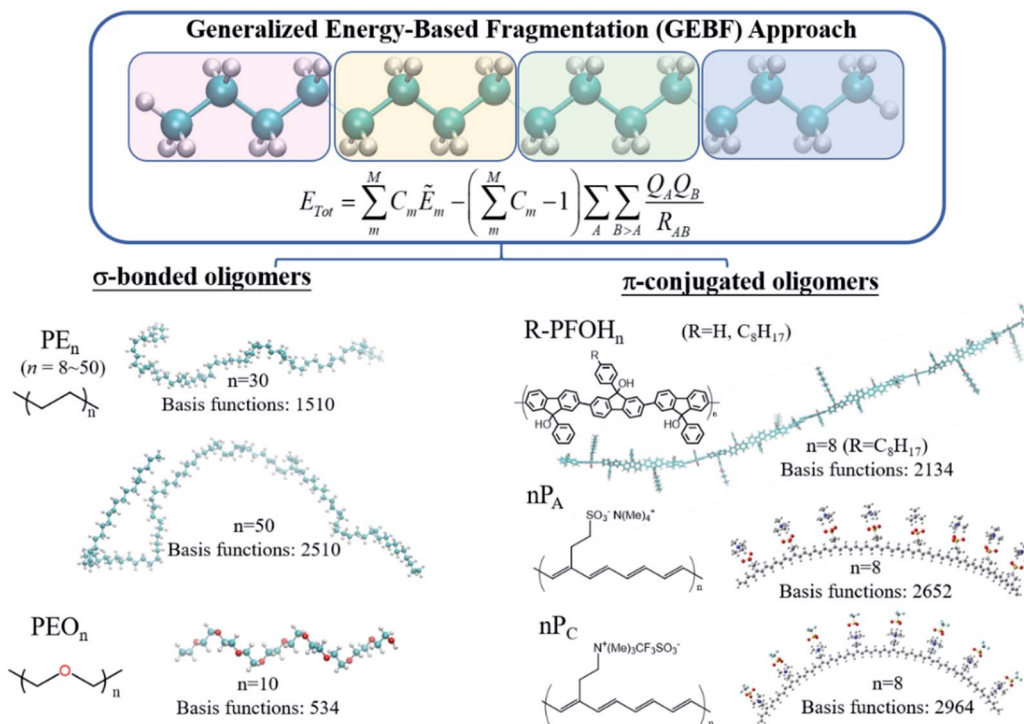


Fig. 3 Illustration of the GEBF method and its application to long polymer oligomers.

be represented as the linear combination of the corresponding energy (or energy derivatives) of a series of electrostatically embedded subsystems (Fig. 3). In fact, this is a very crucial step in making the linear-scaling fragmentation method applicable to material systems, since many functional materials are highly polar or charged and hence responsive to the stimuli of electric, light, pH and temperature changes. By improving the fragmentation schemes or the constructions of subsystems, the GEBF approach was further applied to a broad range of complex systems with polar or charged groups including polymer oligomers, molecular clusters, ionic liquid clusters, biological systems, and supramolecular complexes.^{82,83} Other energy-based fragmentation methods, such as the generalized MFCC method,^{84,85} the molecular tailoring approach,⁸⁶ the molecules-in-molecules (MIM) method,⁸⁷ the generalized many-body expansion method,⁸⁸ have also been developed. To better correlate with experimentally observable properties, the energy-based approaches have been applied to study the relative stabilities and molecular spectroscopic properties (IR/Raman and NMR spectra) of large systems at the levels of HF, DFT, and post-HF methods.^{73,82,83,89,90}

The electronic structure calculations of condensed-phase systems (such as solids, surfaces, and liquids) play important roles in materials science. However, the traditional periodic DFT calculations using plane waves (or Gaussian-type atomic orbitals), which are widely used for condensed phase systems, are much more expensive than the non-periodic DFT calculations of molecules or clusters with similar sizes due to the large number of Bloch vectors under PBCs. On the other hand, due to the dependence of exchange-correlation functionals, DFT

calculations may not be accurate enough to describe the relative stabilities of polymorphs, which are usually in the range of 1–2 kcal mol⁻¹. *Ab initio* electron correlation methods could systematically provide more accurate relative energies. However, periodic electron correlation methods are extremely expensive and are only applicable to model condensed phase systems with several small molecules in a unit cell, even for the PBC-MP2 method. Using the localized Wannier functions in the occupied space, local correlation methods were applied to periodic systems. Those methods include the incremental method,⁹¹ the local MP2 method,⁹² the divide-expand-consolidate method,⁹³ the PBC-CIM method,⁹⁴ and so on. In the PBC-CIM method developed in our group, the correlation energy per unit cell of a periodic system can be expressed as the summation of the correlation contributions of occupied orbitals within a series of finite-sized clusters.⁹⁴ Fragmentation methods have also been extended to periodic systems. In such methods, the unit cell energy of a periodic system could be represented as the summation of *n*-fragment (*n* = 1, 2, ...) energy terms, which could be approximately obtained from the calculations on finite molecular clusters. For instance, the systematic molecular fragmentation and hybrid many-body interaction model could predict the lattice energies or lattice structures of covalent crystals or organic molecular crystals.^{216,217} A fragment-based QM approach has been used to estimate the lattice energy of benzene crystals at a high-level electron correlation level.⁹⁵ To take the long-range electrostatic interactions in the infinite crystal environment into account, we have developed a PBC-GEBF method.^{96,97} In the approach, the ground-state energy or energy derivatives of

a periodic system can be evaluated as a linear combination of ground-state energies or energy derivatives of various small nonperiodic subsystems. Here, each subsystem is embedded in the electric field generated by a finite array of background point charges. The PBC-GEBF approach could be employed to predict the lattice energies, crystal structures, and spectroscopic properties of various molecular materials and solutions at various DFT and electron correlation levels.⁸³

Besides the above-mentioned linear scaling DFT and wavefunction-based methods, semiempirical QM methods could also greatly speed up QM calculations by using some empirical parameters to save the computation time of evaluating two-electron integrals. The widely used semiempirical QM methods include Austin model 1 (AM1),⁹⁸ parametric method 6 (PM6),⁹⁹ DFT tight-binding methods such as density functional tight-binding (DFTB)^{100,101} and extended tight-binding (*x*TB)¹⁰² methods. Furthermore, linear scaling semiempirical QM methods could be applied to treat even larger systems. For example, the FMO method has been implemented at the level of DFTB with the third-order expansion (DFTB3), called FMO-DFTB3, which is more than 40 times faster than full DFTB3 for calculating a cellulose sheet containing 1368 atoms.¹⁰³ Nakai and co-workers have developed the DC-DFTB method for the on-the-fly molecular reaction dynamics simulations of a cubic water box with 256 000 water molecules.¹⁰⁴

2.2 Low scaling excited-state quantum mechanics and quantum dynamics methods

The fundamental physics and chemistry of many optical functional materials ranging from optoelectronic devices to photocatalysts are governed by light initiated excited-state processes, including photon absorption, radiative and radiationless relaxation, excited-state energy transfer, excited-state charge transfer, *etc.* Understanding the properties of electronically excited states is impossible to be accomplished without valuable help from quantum chemical and quantum dynamics calculations. However, these theoretical methods for electronic excited states are usually very expensive because their computational costs grow even much faster with the increasing system size than that of ground-state quantum chemical calculations. The upper limit for the applicability of the most common excited-state electronic structure method, time-dependent density functional theory (TDDFT), or even simpler configuration interaction singles (CIS) method, if no further approximations are introduced, is only about 150–200 atoms.¹⁰⁵ Therefore, the high demand for interpreting experimental excited-state phenomena and the recent fascinating progress in time-resolved spectroscopy called for the development of novel excited-state theoretical methods for large systems, which was an active research field of quantum chemistry in the last decade.

One of the widely used strategies to reduce the costs of excited-state calculations is to utilize local excitation approximation (LEA), in which electronic excitation is restricted to only one specified chromophore. By using various types of localized molecular orbitals, including regional LMOs (RLMOs), natural transition/localized orbitals and absolutely LMOs (ALMOs), to

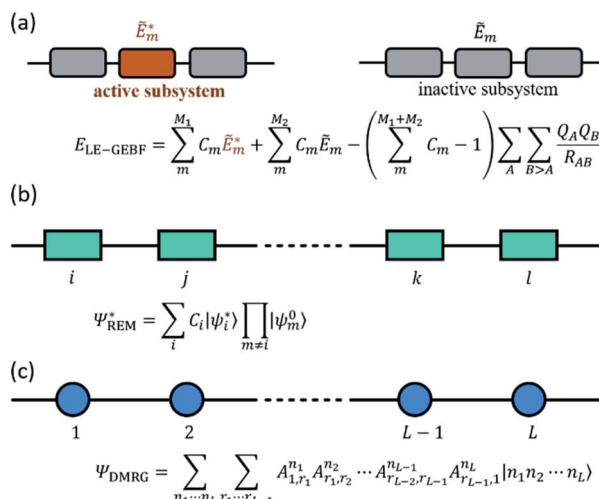


Fig. 4 Schematic illustration of (a) LE-GEBF subsystems, (b) REM wavefunction, and (c) DMRG wavefunction. The rectangle in (b) denotes a molecular fragment or block and $|\psi_i^0\rangle$ and $|\psi_i^*\rangle$ are the wavefunctions of its ground and excited states respectively with C_i being the configuration coefficient. The circle in the bottom denotes a molecular orbital or a vibrational mode, and $|n_i\rangle$ represents its local basis with A^{n_i} being MPS matrices.

constrain the spatial region of the local excitation, LEA was successfully implemented at the levels of TDDFT and CIS.^{106–109} In recent years, the great success of linear-scaling fragmentation-based approaches in describing the ground-state also motivated its straightforward extension to excited-state calculations through a combination with LEA.^{18,110,111} As shown in Fig. 4a, Li *et al.* also extended the GEBF method to the local excitation GEBF (LE-GEBF) method.^{83,111} In this method, the localized excited-state energy of a target system can be represented as the combination of the excited-state energies of active subsystems and the ground-state energies of inactive subsystems with an overcounting correction of electrostatic interactions. The LE-GEBF method is employed to describe the solvatochromic shifts of acetone in different solvent environments and the electron absorption spectra of green fluorescence protein (GFP).^{83,111} Besides the above mentioned fragmentation schemes, the embedding algorithms which incorporate a high-level calculation in the active region of interest and a low-level calculation on its environment are also employed for unravelling the excited-state properties of large systems such as GFP.¹¹² Recently, quickly developed machine learning techniques were also suggested by Chen *et al.* to be used to further reduce the computational costs of low-level quantum chemical calculations of the large inert regions surrounding the photochemically active space in embedding algorithms.¹¹³

Another widely used strategy for low-scaling ground-state calculations, local correlation approximation (LCA), is also applied for describing the excited states of large systems. Taking advantage of the locality of a reduced density matrix gained by the DC method, linear scaling was achieved for TDDFT by using orthogonal atomic orbitals (OAOs) or non-



orthogonal LMOs (NOLMOs).^{114,115} Liu and coworkers¹¹⁶ later developed another linear-scaling TDDFT scheme by making full use of a simple pre-screening of the particle–hole pairs in the fragment LMO (FLMO) representation. Similarly, LCA has been also incorporated into various wavefunction theory (WFT) methods, such as equation-of-motion CCSD (EOM-CCSD),¹¹⁷ second-order approximate coupled-cluster singles and doubles (CC2),¹¹⁸ multi-reference singles and doubles configuration interaction (MRSDCI),¹¹⁹ and CIS¹²⁰ as well as symmetry adapted cluster configuration interaction (SAC-CI).¹²¹ Nakai and coworkers used standard DC-based approaches to evaluate the dynamical polarizability and then described the excited states as the poles of dynamical polarizability.^{122,123} It has been successfully implemented from the TDDFT level to the coupled cluster linear response (CCLR) level.

At the same time, excitonic models are often used in computational materials science or photochemistry for the qualitative/semi-quantitative investigation of various optoelectronic processes in condensed phases, ranging from photo-absorption/emission, excited-state energy transfer to singlet exciton fission and exciton dissociation.^{124–131} However, the choice of the parameter values in the excitonic models is usually dependent on the experimental fitting or simple quantum chemical estimation for classical coulombic electrostatic interactions between different chromophores. Obviously, the construction of the excitonic model is non-trivial when each chromophore has more than one excited state involved in the system's optoelectronic process or the short-distance inter-chromophore exchange interaction is non-negligible, and this will greatly decrease the accuracy of the model and also severely restrict the model's application range. In order to better describe the inter-chromophore interactions, Bloch's effective Hamiltonian theory¹³² can be adopted in conjunction with the numerical renormalization group (NRG) for large correlated systems. Using this strategy, Morningstar and Weinstein¹³³ proposed the contractor renormalization group (CORE) method, in which the general excited-states of the whole system are considered as an assembly of numerous single or multiple local block excitations, and Malrieu and coworkers¹³⁴ suggested the renormalized excitonic model (REM) to approximate the whole system's low-lying excited states as linear combinations of only single local excitations (Fig. 4b). With this approximation, the dimensions of the effective Hamiltonian matrix of the whole system can be reduced greatly from d^N to $d \times N$, where d is the number of local states and N is the total number of blocks. Since 2012, our group has been implementing REM at the *ab initio* level in conjunction with full CI (FCI), CIS, SAC-CI and TDDFT using orthogonal LMOs (OLMOs) and block canonical molecular orbitals (BCMOs).^{135–137} The tests of hydrogen chains, polyene, polysilenes, water chains, and benzene aggregates as well as general aqueous systems with polar and nonpolar solutes indicate that the *ab initio* REM method can give good descriptions of excitation energies for the lowest electronic excitations in large systems with economic computational costs.

On the other hand, the accurate theoretical interpretation of ultrafast time-resolved excited-state spectroscopy experiments

relies on full quantum dynamics simulations for the investigated system, which is also computationally prohibitive for realistic molecular systems with a large number of electronic and/or vibrational degrees of freedom. To tackle this so-called curse of dimensionality, many low-scaling quantum dynamics methods using different approximations have been proposed. Among them, tensor product methods¹³⁸ recently attracted much research interest. For example, MCTDH²³ adopts a Tucker decomposition¹³⁹ scheme to decompose a high-order tensor with a high rank into a set of matrices and one small Tucker core tensor with the same order but a low rank, and accordingly it can be also considered as a high-order single value decomposition (HOSVD).¹⁴⁰ However, the Tucker core still suffers from the curse of dimensionality for higher orders, which has been partly overcome by introducing multi-layer MCTDH (ML-MCTDH)¹⁴¹ using a hierarchical Tucker (HT) decomposition. On the other hand, the tensor train decomposition (TT; in the mathematical literature)¹⁴² or the equivalent matrix product state representation (MPS; in the physical literature)¹⁴³ used in the density matrix renormalization group (DMRG)^{144,145} provides an alternative decomposition algorithm, which decomposes a high-order tensor with a high rank into a product of many local low-order tensors with a one-dimension (1D) topology (Fig. 4c). ML-MCTDH and tDMRG²² have been successfully applied to simulate the dynamics of excited-state energy or charge transfer and the absorption and fluorescence spectra of molecular aggregates,^{26,27,146–152} demonstrating the great potential for exploring the quantum dynamics of excited-state processes in large chemical systems.

In addition, there also exist various semiempirical excited-state QM methods, such as time-dependent DFTB (TDDFTB) method¹⁵³ and *x*TB based simplified Tamm–Dancoff approximation (sTDA-*x*TB) method.¹⁵⁴ A spin-flip TDDFTB (SF-TDDFTB) method is developed to fast determine S_0/S_1 minimum energy conical intersection (MECI) structures.¹⁵⁵ In 2019, Nakai and co-workers implemented a GPU-accelerated DC-TDDFTB method, which could reproduce the experimental absorption and fluorescence spectra of 2-acetylindan-1,3-dione in explicit acetonitrile solution.¹⁵⁶

It is not straightforward to precisely compare the accurate and costs of various low scaling QM methods because there usually exist some adjustable parameters for achieving the balance between the accuracy and computational costs. Also, those methods may show different performances for various types of large subsystems. Collins and Bettens have made some comparisons between several typical energy-based fragmentation methods in their review.⁷³ It shows that the absolute errors in the total energies are usually several kJ mol^{-1} for medium-sized systems and more than 10 kJ mol^{-1} for large-sized systems such as proteins. By taking the long-range electrostatic interactions into accounts, the computational accuracies are improved for a broad range of large systems, especially for polar or charge systems. Furthermore, for the relative energies (such as binding energies or reaction barriers), which are of chemical interest, the errors are smaller due to the error cancellation. For example, for ten host–guest complexes, the maximum error of the GEBF-DFT binding energies is only



4.4 kJ mol⁻¹, and the maximum error for the relative binding energy between two complexes with the same host molecules is only 0.9 kJ mol⁻¹.¹⁵⁷ In local correlation methods, there are some direct comparisons for same large systems.^{158,159} For example, Li and co-workers have compared resolution-of-identity MP2 (RI-MP2) and CIM-RI-LMP2 methods, which shows that the CIM approach gives better accuracies and efficiencies for quasi one-dimensional peptides.¹⁵⁸ Neese and co-workers have compared the accuracies and efficiencies between the domain based local pair-natural orbital (DLPNO) and CIM calculations at the MP2 and CCSD(T) levels for large systems up to 2380 atoms.¹⁵⁹ It shows that their efficiencies are similar, while the DLPNO total energy is more accurate for 3-dimensional systems. For a tight CIM parameter, the accuracies of CIM and the DLPNO energy are very close.¹⁵⁹ In addition, the fragmentation or local correlation methods are developed to reproduce the corresponding traditional QM methods, and thus their accuracies also depend on the levels of DFT or electron correlation methods. In comparison with “first-principles” DFT methods, DFTB is a semiempirical DFT-based method and additional empirical dispersion corrections need to be added for systems with weak interactions.¹⁰¹

Codes of low scaling ground- and excited-state QM methods are developed by several groups and available in several packages. Some packages are specifically designed for low scaling QM methods, such as ONETEP¹⁶⁰ and HONPAS¹⁶¹ based on localized Wannier functions, LSQC¹⁶² (including GEBF and CIM), *etc.* In addition, some low scaling methods, such as FMO, DC, and CIM, are available in the exited GAMESS package;¹⁶³ local MP2 and CCSD(T) are implemented in the Molpro program;¹⁶⁴ DLPNO and CIM methods are included in the ORCA program.¹⁶⁵ For periodic systems, low scaling DFT codes are available in Crystal,¹⁶⁶ CP2K,¹⁶⁷ *etc.* The specific packages for DFTB, such as DFTB+¹⁶⁸ and xTB,¹⁰² were also widely used to predict the energy and properties of some complicated systems.

3 Applications of low scaling QM methods to complex molecular material systems

In this section, some applications of the methods mentioned in Section 2 are discussed. A thorough overview of the several hundred or even more applications of applying low-scaling QM methods and ML to molecular materials is certainly out of the scope of this review. Also, there exist many methods for inorganic or nanomaterials. As early as 2014, Yang and co-workers have employed a density matrix trace correcting (TC) purification method to compute various electronic properties of hexagonal graphene nanoflakes with up to 11 700 atoms.¹⁶⁹ Recently, Hu and co-workers have applied pole expansion and selected inversion (PEXI) to calculate the electronic structures of boron nitrogen nanotubes.¹⁷⁰ Our aim is not only to show the potential and applicability of different methods and techniques and, by discussing some representative calculations, but also to help the reader to select an appropriate approach for particular molecular material systems.

3.1 Polymeric oligomers

Fragmentation based linear scaling methods can treat polymeric oligomers in a direct and economic way. For σ -bonded oligomer chains, such as the widely used polyethylene (PE) and poly(ethylene oxide) (PEO) systems, each repeat unit or several repeat units can be taken as a fragment (Fig. 3).^{44,171} Such a fragmentation scheme also works well for the π -conjugated chains like polyacetylene and polyfluorens but the π -bonds cannot be cut during the fragmentation.^{172,173} An auto fragmentation program was implemented for more complicated molecular aggregate or biological systems with a pre-setting truncate distance for building the subsystems in GEBF calculations.¹⁷⁴

The combined quantum mechanics and molecular mechanics (QM/MM) method is an efficient method for studying macromolecules in solutions, in which the solute is usually treated by the QM method. The high computational scaling of the QM method is still a bottleneck of QM/MM simulations for macromolecules which require a large QM region. To overcome this difficulty, we have developed a fragment QM/MM method by combining GEBF-based QM and MM calculations for the Born–Oppenheimer molecular dynamics simulations of dilute solutions of macromolecules.¹⁷¹ As for the two selected representative systems, PEO is a water-soluble polymer with extensive industrial applications, and PE is a very important polymer in the plastic industry. GEBF-based QM/MM optimization and MD simulations were performed for PEO_n ($n = 6$ –20) and PE_n ($n = 9$ –30) in aqueous solutions. As expected, the longer oligomer chains have larger chain flexibility and curling occurs in some local parts of the long σ -bonded oligomer chains.¹⁷¹

π -Conjugated polymers are relatively more rigid than σ -bonded oligomers. The high extent of electron delocalization in π -conjugated aromatic rings brings about the unique optical and electronic properties of various functional material molecules. In addition, the highly directional noncovalent interactions play important roles in the self-assembly behaviour of π -conjugated polymers to fabricate organogels and thin films. We take oligofluorens, (R)-PFOH_n ($n = 4$ and 8) where R = H (unsubstituted) or OC₈H₁₇ (substituted), for side chains as an example. GEBF-B3LYP with the 6-31+G(d) basis set was employed to optimize the oligofluorens.¹⁷³ Furthermore, the packing structures for (R)-PFOH_n in crystals, amorphous solids and solutions were investigated by polymer consistent force field (PCFF) based MD simulations. Then, for the MD sampled configurations, the ultraviolet/visible (UV/VIS) absorption spectra were computed by the TDDFT and FLMO based TDDFT (FLMO-TDDFT) method.¹¹⁶ The results show that the planar π -conjugated conformations could lead to a red shift in the absorption spectra upon increasing the concentration of solution. The aggregation-induced red-shift of oligofluorens and the blue-shift of oligothiophenes were rationalized in a unified way.¹⁷³ Aggregated-configuration engineering could be used to tune the optical properties of electronic devices based on π -conjugated systems.

As mentioned before, the introduction of background point charge into subsystem calculations allows GEBF to give accurate



results for charged or highly polar molecules. It can be demonstrated by its application to ionically functionalized polyacetylene analogues, such as poly(tetramethylammonium 2-cyclooctatetraenylethanesulfonate) (**P_A**) and poly[(2-cyclooctatetraenylethyl)trimethylammonium trifluoromethanesulfonate] (**P_C**), which acted as active materials sandwiched between two electrodes (gold nanoparticles). It is very useful in the fabrication of various microelectronic devices, such as light-emitting electrochemical cells and electric current rectifiers. In such devices, the polymer/electrode and polymer/polymer interfaces are really complicated for theoretical simulations. We have combined linear scaling DFT calculations and molecular dynamics (MD) simulations to study the unusual transport properties of an Au|**P_C**|**P_A**|Au junction.¹⁷² The energy-based fragmentation approach at the B3LYP/6-31G(d) level was used to optimize the structures of the ionically functionalized oligomers, **nP_A** and **nP_C** ($n = 1-8$). The all possible *cis*-configurations of 8P_A and 8P_C, with the counter ions residing on the same sides of the polyacetylene backbones, are displayed in Fig. 3. Through the oligomer extrapolation of the highest occupied molecular orbital (HOMO) and the lowest unoccupied molecular orbital (LUMO) energies of **nP_A** and **nP_C** as a function of $1/n$, the valence band (VB) and conduction band (CB) edges of **P_A** and those of **P_C** were estimated, which are in qualitative agreement with the PBC calculation results.¹⁷² The absence of n-doping waves in the voltammetry data of **P_A** in the experiment is rationalized by its high reduction potential or the blocking of effective interfacial electron transfer.

For other oligomers, many density-matrix based or fragment-based linear scaling methods have been employed. For example, Liang and Chen and co-workers have extended the localized-density-matrix (LDM) method for the calculations of nonlinear optical responses (second hyperpolarizability) in large polyacetylene oligomers.¹⁷⁵ Kobayashi and Nakai have developed DC-HF and DC-MP2 methods for delocalized or open-shell systems by determining the electrons automatically with a universal Fermi level. Using the approach, the energies of the B-N analogues of oligoacenes (BN-acenes) and their derivatives are comparable with the corresponding conventional values.¹⁷⁶ Skylaris and co-workers have used linear scaling DFT in the ONETEP program¹⁶⁰ to compute the HOMO and LUMO energies, and the band gap of some long chain oligomers of organic photovoltaics with more than 1000 atoms.¹⁷⁷

3.2 Supramolecular complexes and molecular aggregates

Two-dimensional self-assembled monolayers and supramolecular complexes are important ingredients in the construction of novel smart electronic devices. The packing structures and properties of those molecular aggregates are controlled by non-covalent interactions, whose strength could be calculated by low-scaling QM methods. There are numerous application examples in this direction. Here, we just list some calculation results. Pentacene (Pn) and its functionalized derivatives are widely used building units in high-performance organic thin-film transistors and organic photovoltaics. We have computed the GEBF-MP2 binding energies, E_b , of a series of pentacene (Pn)_N aggregates, with up to

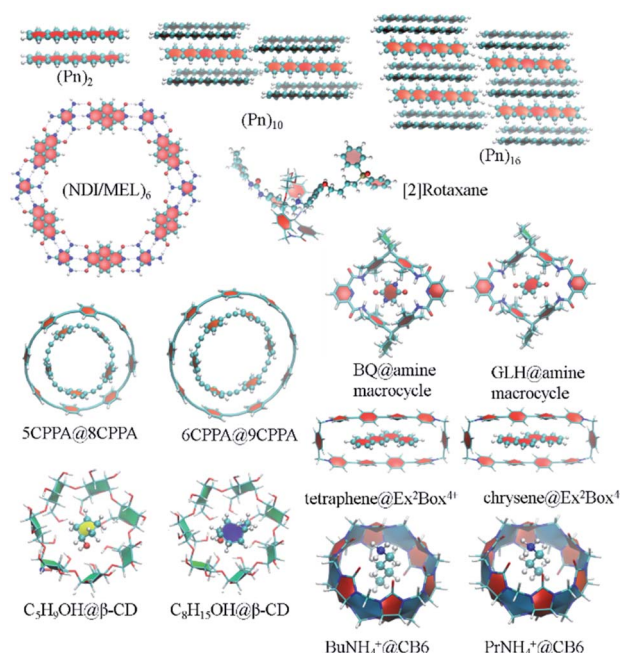


Fig. 5 Some supramolecular complexes, which were studied by the GEBF approach for binding energies, including (Pn)_N oligomer ($N = 2, 10, 16$), (NDI/MEL)₆, [2]rotaxane, 5CPPA@8CPPA, 6CPPA@9CPPA, BQ@amine macrocycle, GLH@amine macrocycle, C₅H₉OH@ β -CD, C₈H₁₅OH@ β -CD, tetraphene@Ex²Box⁴⁺, chrysene@Ex²Box⁴⁺, BuNH₄⁺@CB6, and PrNH₄⁺@CB6.

Pn hexadecamer ($N = 16$), with the 6-31G(d) basis set (Fig. 5).¹⁷⁸ In the (Pn)₁₆ aggregate, the van der Waals and π -stacking interactions are dominant in the non-covalent binding with an E_b of -20.54 kcal mol⁻¹. In contrast, the molecular aggregates with favourable hydrogen bonding (HB) networks usually have larger binding strength. Such a kind of directional HB intermolecular interaction could drive the formation of various packing patterns, such as honeycomb networks, chessboard, and chiral supramolecular structures on the surface or in solutions (Fig. 5). Taking the naphthalene tetracarboxylic di-imide (NDI) and melamine (MEL) binary system as an illustration, these two kinds of π -conjugated molecules constitute a pair of building blocks for constructing hexagonal close-packed architectures. The counterpoise-corrected binding energy of the hexagonal NDI/MEL network including six pairs of NDI/MEL dimers, (NDI/MEL)₆, is predicted to be -297.8 kcal mol⁻¹ by GEBF-MP2/6-31G(d) calculations. The triple hydrogen-bonded network is consistent with the image from the scanning tunnelling microscope (STM) on the gold surface.¹⁷⁹

In addition, the non-covalent interactions of supramolecular host-guest complexes are the driving forces of the supramolecular recognition and self-assembly formation. As a kind of mechanically interlocked molecule being used in molecular devices or nanoscale machines, [2]rotaxane is a \langle rod|ring \rangle system consisting of a rod (an axle-shaped molecule) and a ring (a macrocyclic compound). The difference in the HB interaction energies between the macrocycle and different binding sites in the long rod of [2]rotaxane is employed to control the shuttling movement.⁴² In order to accurately predict the binding energies



of the supramolecular complexes, we have proposed an efficient way for the constructions of GEBF subsystems to avoid the selection of the whole macrocycle in terms of the cut-off distance from the central guest species.¹⁵⁷ In the new scheme, each large primitive subsystem is converted into several overlapped smaller primitive subsystems using an iterative algorithm. Then, the primitive GEBF subsystem for a supramolecule is smaller than before to achieve similar accuracy, and the subsystems in the complex are very similar to those in the host. Thus, more accurate binding energies could be obtained with smaller but consistent subsystems.¹⁵⁷ We have performed GEBF-M06-2X calculations for ten host-guest complexes taken from the S30L dataset,¹⁸⁰ including [5]cycloparaphenylenecetylene (5CPPA) in 8CPPA and 6CPPA in 9CPPA, benzoquinone (BQ) and glycine anhydride (GLH) in the amine macrocycle, cyclopentanol (C_5H_9OH) and cyclooctanol ($C_8H_{15}OH$) in β -cyclodextrin (β -CD), tetraphene and chrysene in the Ex^2Box^{4+} macrocycle, and protonated butylammonium ($BuNH_4^+$) and propylammonium ($PrNH_4^+$) in cucurbit[6]uril (CB6) (parts of which are listed in Fig. 5).¹⁵⁷ The GEBF approach could reproduce the conventional DFT binding energy and relative binding energy (for two complexes with the same or similar hosts) with the errors being less than 1 kcal mol⁻¹ and 1 kilojoule mol⁻¹, respectively.

In addition to binding energies and packing structures, property predictions are highly desired for bridging the gap between theoretical simulations and experimental measurements of molecular aggregates. By combining GEBF-based *ab initio* MD (AIMD) and polarizable force field (polar FF)-based MD simulations with variable charges, we investigated the conformational changes and averaged NMR chemical shifts of [2]rotaxane in solution.⁴² The up-field shifts of NMR signals of rod H-donors are induced by the dipole-dipole interactions between the flexible diethylene glycol chain of the ring and polar acetonitrile solvents, which also leads to the inhomogeneous and directional distribution of the neighbouring solvents. This implies that the interactions between the guest and host or between solvent and solute play an important role in designing novel interlocked systems.⁴² Recently, in order to treat large systems in solution, the GEBF approach was combined with a universal solvation model based on solute electron density (SMD). The GEBF-SMD approach could compute the solvation energies or predict the relative energies of large systems in solutions.¹⁸¹ In addition, Ochsenfeld and coworkers have employed a linear scaling DFT method to investigate the influence of intra- and intermolecular interactions on the NMR chemical shifts of supramolecular complexes, in which a naphthalene-spaced tweezers molecule is taken as the host with various aromatic, electron-deficient guests.¹⁸²

Vibrational circular dichroism (VCD) spectra are useful to determine the chiral molecules by the analysis of differential absorption between left- and right-circularly polarized infrared radiation. The conventional QM calculations for the VCD spectra of MD sampled molecular aggregates in amorphous solids or solutions are limited to medium-sized clusters. The GEBF approach was implemented to compute the VCD spectra of (*S*)-alternarlactam aggregates at the B3PW91/6-31+G(d,p) level, where the VCD signals are obtained from the rotational

strength of the GEBF subsystems.¹⁸³ Hydrogen-bond interactions dominate in the packing configurations at a low density (0.5 g cm⁻³), and the GEBF calculated VCD spectrum is in good agreement with the experimental result, with signal splitting in C=O stretching vibrational regions.¹⁸³

Another kind of low scaling method, the CIM approach,^{61,62} has also been applied to calculate the binding energies of various supramolecular complexes, metal-containing molecular aggregates and zeolites (Fig. 6).^{60,64} For example, the CIM-MP2 relative energies of different L-amino acid ethyl ester hydrochlorides (*L*-AA-OEt) in water-soluble pillar[5]arene WP5 were obtained to describe different chiral conformations.¹⁸⁴ To understand the mechanism of a chemically self-charging aqueous zinc-organic battery, which consists of a poly(1,5-naphthalenediamine) (*i.e.*, poly(1,5-NAPD)) cathode, a Zn-foil anode and an alkaline electrolyte, the binding energies of (1,5-NAPD)₇ with different ions (H^+ , Zn^{2+} , and K^+) were calculated by CIM-RI-MP2 with the def2-TZVPD basis set.¹⁴ The high level CIM-DLPNO-CCSD(T) binding energies were also obtained for a molecular capsule with multiple hydrogen interactions. With this binding energy as a reference, the results show that several DFT functionals overestimate the binding energies. The binding ability of trapping ethanol molecules in a ZSM-5 zeolite cage is evaluated by CIM-DLPNO-CCSD(T) calculations, which indicates that the M06-2X functional could provide an

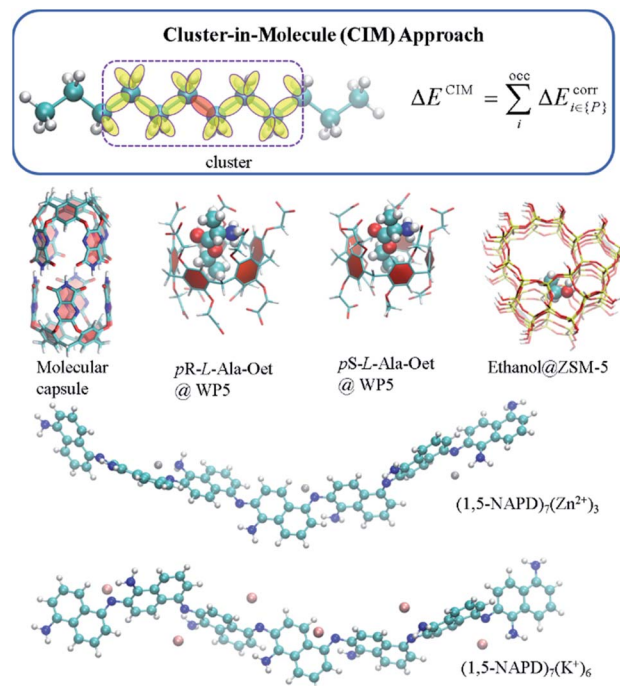


Fig. 6 The cluster-in-molecule approach and some studied supramolecular complexes. On the top, a cluster is represented in a dotted rectangle, in which the central and environmental localized molecular orbitals are denoted in red and yellow, respectively. The studied supramolecular complexes include a molecular capsule, two L-alanine ethyl ester hydrochlorides (*pR*-L-Ala-Oet and *pS*-L-Ala-Oet) in water-soluble pillar[5]arene (WP5), ethanol@ZSM-5 zeolite, and two clusters in a chemically self-charging aqueous zinc-organic battery, (1,5-NAPD)₇(Zn²⁺)₃ and (1,5-NAPD)₇(K⁺)₆.

reasonable binding energy.⁶⁴ In another way, Jorgensen and co-workers have applied their Massively parallel divide-expand-consolidate RI-MP2 (DEC-RI-MP2) to 1-aza-adamantane-trione (AAT) supramolecular wires including up to 2440 atoms and 24 440 basis functions.¹⁸⁵ Raghavachari and co-workers have employed a multilayer MIM method to study of the energies of foldamers and their complexes with anions. It demonstrates that a two-layer MIM2 model, in which DLPNO-CCSD(T) and DFT with Grimme's dispersion correction (DFT-D3) methods are employed as high and low levels, respectively, could provide accurate binding energies by taking long-range interactions into account.¹⁸⁶

To sum up, the improvement of fragmentation schemes and the employment of local correlation methods could yield accurate binding energies of large-sized supramolecular complexes and molecular aggregates at the electron correlation levels.

3.3 Stimuli-responsive monolayers

The ordered self-assembly of molecular monolayers on the surface plays an important role in molecular electronics, photonics, and optical devices. The introduction of stimuli-responsive groups into monolayers is an efficient way to fabricate novel smart sensors and drug release systems.^{41,187-191} An electric field could trigger the moment of the charged head groups or molecular chains of monolayers deposited on substrates. In some cases, the charged oligomer chains are polarized under the electric field. The polarizable force fields are desired to give reasonable descriptions of the electric field driven switching process. GEBF was able to provide variable partial charges or fragment dipoles in response to the conformational changes.

As shown in Fig. 7, the energy-based fragmentation method was used on biotin-4KC, *i.e.*, a positively charged tetramer of lysine (K) that is functionalized at one end with the bioactive moiety biotin, which could bind with the neutravidin protein, and at the other end with a cysteine (C), for binding to gold substrates. An electro-switchable surface can be formed by a binary mixed monolayer with biotin-4KC and a short chain of an ethylene glycol-terminated thiol (*i.e.* (3-mercaptopropyl)tri(ethylene glycol), TEGT), which could fill the space around the biotin-4KC and give enough room for biotin-4KC to switch its backbone under electric field stimuli. Based on the response of a charged molecular backbone of biotin-4KC in such a mixed self-assembled monolayer (SAM), the binding activity of a ligand (biotin) to a protein (neutravidin) can be dramatically changed. It was found that when an upward electric potential (+0.3 V) was applied, high neutravidin protein binding was observed (called ON), while the application of a downward potential (-0.4 V) gave rise to the OFF state with a minimal protein binding ability. Under open circuit (OC) conditions, the protein binding capability was intermediated, lying between the ON and OFF states. The electrostatic potential surfaces of OC, ON, and OFF states indicate the high polarization of charge distribution of the charged biotin-4KC chain under an external electric field. The biotin-4KC chain can be cut into five

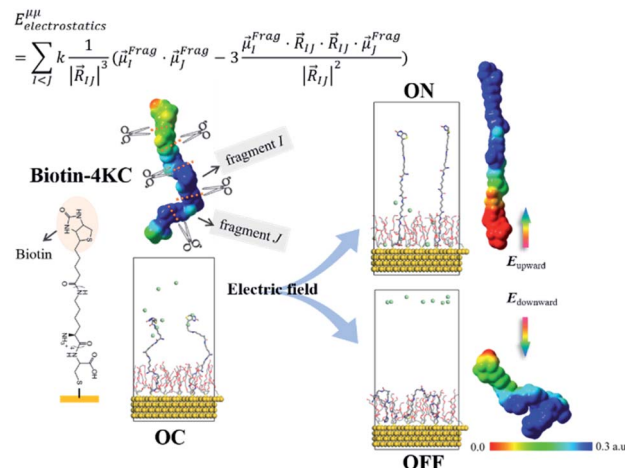


Fig. 7 Polarization model for evaluating electrostatic interaction energy with variable electrostatic parameters such as fragment-based dipole moments coming from the fragmentation QM calculation and its application to the simulation of a stimuli-responsive biotin-4KC monolayer on gold surfaces under three different conditions: without an external electric field (OC), upward (ON), and downward (OFF) electric fields.

fragments according to its constituent groups with each fragment containing a lysine or biotin group, which is called fragment I or fragment J, without the loss of generality. For MD sampled configurations, the GEBF-M06-2X calculations were carried out on-the-fly to provide partial charges or fragment dipole moments in a coarse-grained way for polarized force field simulations. For example, the electrostatic interaction energy could be calculated from the dipole-dipole interaction, $E_{\text{electrostatics}}^{\mu\mu}$, between any two fragment dipoles, $\vec{\mu}_i^{\text{Frag}}$ and $\vec{\mu}_j^{\text{Frag}}$, as shown at the top of Fig. 7. The updated electrostatic interaction energy is used to replace the fixed charge electrostatic term in the traditional force field. It can be found from Fig. 7 that the application of polarizable force field simulations under upward and downward electric fields, respectively, demonstrated the standing straight up (ON) and bending down (OFF) of the biotin-4KC chain, reproducing well the experimental observations.¹⁸⁹

Polarizable FF models were also applied to simulate the macrocyclic ring at different binding states of [2]-rotaxane, each of which is set as the initial state for GEBF-M06-2X based AIMD simulation to efficiently cut down the computational costs and improve the performance of AIMD simulations.⁴²

3.4 Excited state processes in molecular aggregates

One of the most fundamental issues in discussing about the excited processes in molecular aggregated systems is to accurately describe their absorption and emission spectra, which requires an electronic structure calculation of excited states and/or a Fourier transformation of time correlation functions from a quantum dynamics simulation. In 2014, Ma and Troisi²⁰ predicted direct photo-generation of long-range charge transfer (CT) states in organic photovoltaics through a simulation of the absorption spectra at a tetracene/perylene-3,4,9,10-



tetracarboxylic dianhydride (PTCDA) interface by using the REM approach. This was later verified by the experimental assignment of the full CT state absorption spectrum in micro-crystalline rubrene/C₆₀.¹⁹² Zhang *et al.*¹⁸ employed the electrostatically embedded generalized molecular fractionation (EE-GMF) method, a variant of MFCC, to predict the spectra of a prototype AIE fluorophore: di(*p*-methoxyphenyl)dibenzofulvene (FTPE), nearly reproducing the experimental optical spectra of FTPE in condensed phases.

Applying DMRG into *ab initio* quantum chemistry Hamiltonian can serve as an efficient and computationally accurate method, for describing the excited state electronic structure properties of strongly correlated systems that require large complete active spaces (CASs) composed of up to 100 active orbitals, which are not accessible by conventional multi-configurational WFT methods. For example, in 2014 Sharma *et al.*¹⁹³ computed the individual ground- and excited-state energy levels of [2Fe–2S] and [4Fe–4S] clusters by DMRG calculations with up to 36 active orbitals, suggesting that the low-energy spectrum is very dense due to the presence of many *d*-*d* excited states arising from both orbital transitions and spin recouplings. This finding is later supported by indirect experimental evidence from iron L-edge 2p3d resonant inelastic X-ray scattering (RIXS).¹⁹⁴ In 2019, Cho *et al.*¹⁹⁵ further performed ultraviolet (UV) absorption spectroscopy and stimulated X-ray Raman spectroscopy (SXRS) for [2Fe–2S] complexes, which complement each other by accessing different parts of the electronic spectrum and together can effectively probe the dense *d*-*d* electronic states in the Fe–S clusters. The simulated spectra presented clear signatures of the theoretically predicted dense low-lying excited states within the *d*-*d* manifold. Furthermore, the difference in spectral intensity between the absorption-active and Raman-active states provides a potential mechanism to selectively excite states by proper tuning of the excitation pump, to access the electronic dynamics within this manifold.

In recent years, the quick development of the time-dependent series, such as tDMRG method, also promoted the accurate theoretical simulations of spectroscopy in molecular aggregates, especially for systems with strong electron-vibration/phonon couplings. Ren *et al.*¹⁴⁸ computed the vibronically resolved linear absorption and fluorescence spectra of perylene bisimide (PBI) and distyryl benzene (DSB) aggregates by using tDMRG at zero and finite temperature in conjunction with a Holstein model Hamiltonian. The calculations on PBI molecular chains showed that the practical accuracy of tDMRG reaches that of ML-MCTDH at zero temperature. The comparison with *n*-particle approximation methods on the DSB crystal further shows that tDMRG is not only much more accurate than these approximations but can also practically handle the larger Hilbert spaces arising from increasing the number of vibrational modes to model detailed spectral features. Additionally, it was also shown that appropriate vibronic features in the ultrafast electronic process can be obtained by simulating the two-dimensional (2D) electronic spectrum by virtue of the high computational efficiency of the tDMRG method by Yao *et al.*,¹⁴⁶ by taking an oligothiophene/

fullerene heterojunction as an example. Very recently, Gelin and Borrelli further extended tDMRG to the simulation of the time- and frequency-resolved fluorescence spectra of the Fenna–Matthews–Olson antenna complex at room temperature with an account of finite time-frequency resolution in fluorescence detection, orientational averaging, and static disorder.¹⁹⁶

Unravelling the microscopic ultrafast dynamic conversion processes in photophysics and/or photochemistry depends on an accurate real-time QD simulation. For example, singlet fission (SF) is a spin-allowed photophysical process that generates two triplet excitons from one singlet excited state and has attracted a lot of research efforts in the past decade.^{197,198} In recent years, various low-scaling full QD simulations based on MCTDH, tDMRG, or tensor network state (TNS) have been devoted to the theoretical study of both intermolecular and intramolecular SF processes in different molecular crystals or solutions.^{24,25,199} By employing MCTDH simulations, Tamura *et al.*²⁴ revealed that the slip-stacked equilibrium packing structure in pentacene derivatives enhances ultrafast SF mediated by a coherent super-exchange mechanism *via* higher-lying CT states. By contrast, the electronic couplings for singlet fission strictly vanish at the C_{2h} symmetric equilibrium π stacking of rubrene. In this case, singlet fission is driven by excitations of symmetry-breaking intermolecular vibrations, rationalizing the experimentally observed temperature dependence. In addition, tDMRG simulations were also recently adopted by Li *et al.*²⁰⁰ to obtain a general charge transport picture for organic semiconductors with nonlocal electron-phonon couplings (EPCs). By studying the EPC effect on the carrier mobility, mean free path, optical conductivity, and one-particle spectral function, they located the phonon-assisted (PA), transient localization (TL), and band-like (BL) regimes simultaneously on the transfer integral – nonlocal EPC strength plane. They also identified an intermediate regime, where none of the existing pictures is truly applicable, as a generalization of hopping-band crossover in the Holstein model.

4 Machine learning for molecular materials

The successful applications of low scaling QM calculations and their hybridizations with molecular dynamics simulations in the study of material systems have been collected in the above subsections. Recently, the introduction of various material or QM computation databases and ML methods has changed the traditional “try and error” way to search for novel molecules and materials with desired properties. There are a large number of high throughput screening calculations and ML training and prediction studies for various material systems, and we cannot present all those studies in the review (Table S2†). We only lay emphasis on some selected examples in the three categories of ML methods, *i.e.*, explainable models (with well selected features),²⁰¹ deep learning (with self-learned representations without the predetermined feature characters), and online or transfer learning (with variable training data sets), as shown in Fig. 8.



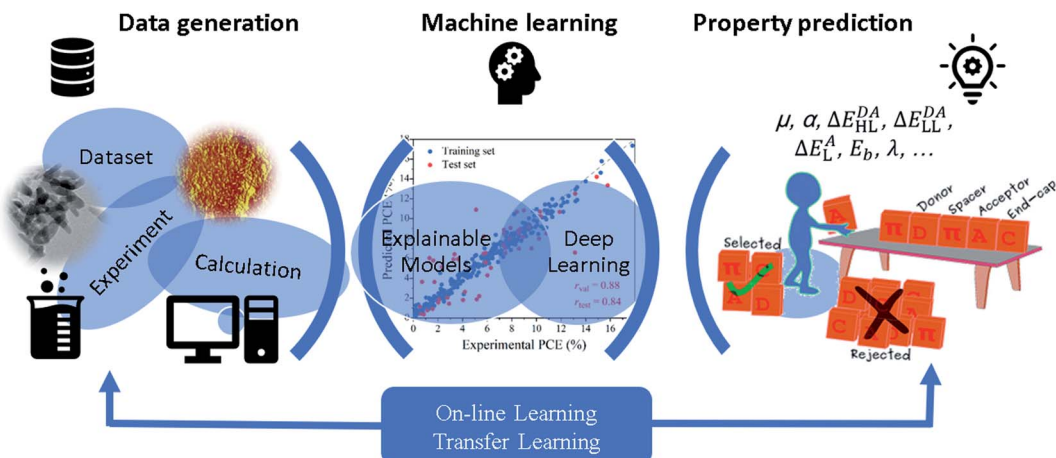


Fig. 8 Schematic illustration of explainable machine learning, deep learning, and on-line or transfer learning methods and their applications to predict molecular or material properties.

Driven by the development of computer science and artificial intelligence, as well as the availability of massive data and efficient data-mining techniques, explainable ML approaches have been widely applied in materials science, with an aim to achieve explainable structure–property relationships with several feature descriptors including structural descriptors (*e.g.*, chain length of oligomers, pore size of zeolites, length/diameter ratio of nanoparticles, *etc.*) and electronic structure descriptors (*e.g.*, dipole moment, polarizability, Frontier molecular orbitals, *etc.*, shown in Fig. 8) without losing the predictive accuracy. For instance, explainable ML models have been learnt to construct QSPR models for predicting different device performances of organic solar cells (OSCs), providing useful suggestions concerning the design of new functional organic materials with desired properties, and contributing to the identification of new OSC materials.^{202–206} In 2018, we identified 13 important structural and electronic structure descriptors to describe 280 donor molecules by in-depth understanding of the microscopic mechanism of OSCs.²⁰⁷ Among them, one is the structural descriptor (number of unsaturated atoms, N_{atom}), while others, such as polarizability, vertical ionization potential, and hole–electron binding energy, are related to the ground- and excited-state properties obtained by quantum chemical calculations. A range of ML algorithms including K-nearest neighbor (KNN), random forest (RF), gradient boosting (GB), and artificial neural network (ANN) were used to construct regression models for predicting power conversion efficiency (PCE). Both tree-based models obtained remarkable predictive power with Pearson's correlation coefficient (r) exceeding 0.78. In addition to improving the overall performance of organic photovoltaics, it is also necessary to meet the other requirements of specific applications for devices, such as high open-circuit voltage (V_{OC}) for solar-fuel energy conversion and high short-circuit current density (J_{SC}) for solar window applications. To this end, we also constructed ML models to predict the other three important device parameters, V_{OC} , J_{SC} , and filled factor.²⁰⁸ On the basis of an extended experimental data set of 300 donor molecules, the predictive accuracy (r) of the GB model for V_{OC} , J_{SC} and filled

factor reached 0.67, 0.66 and 0.71, respectively. Furthermore, we performed high-throughput virtual screening of 10 170 molecules using well-trained ML models.²⁰⁹ All candidates were composed of 32 unique building blocks (four types of units, donor (D), acceptor (A), π -spacer (S) and end-capping (C)) according to ten combinative ways (DA, ADA, DAD, DSA, DSASD, ASDSA, CSDSC, CASDSAC, CDSASDC and CDSAC). In order to derive design rules, an efficient group-combined pair and the most favourable molecular combinations from building blocks were obtained. In addition, the key factors required for highly efficient molecules were clarified. For instance, the energy difference of LUMO+1 and LUMO of donors (ΔL), energy gap ($\Delta H-L$) and N_{atom} of all high-performance dyes have the range of <0.25 eV, <4.25 eV and >60 , respectively. Explainable ML methods have been used in many other kinds of materials, and the readers could find more examples in Table S2.†

The interplay between explainable ML models and experiments is becoming more active. Experimental data are important input to obtain an initial guess of descriptor sets, and conversely, the built explainable QSPR model could help experiments to gain inspiration for constructing the chemical combination space of novel materials and fabrication of materials. For example, a new ML framework for simultaneously optimizing D/A molecule pairs and device specifications of OSCs is proposed.²¹⁰ The structural and electronic properties were further combined with the device bulk properties, which can be measured by atomic force microscope (AFM) experiments. In this way, the built QSPR model achieved unprecedentedly high accuracy and consistency. A large chemical space of 1 942 785 D/A pairs is explored to find potential synergistic ones. Favourable device bulk properties such as the root-mean-square of surface roughness for D/A blends and the D/A weight ratio are further screened by grid search methods. This showed that ML can be effective not only for molecular screening but also for experimental parameter optimization for OSCs, which takes an important step further into the practical theoretical guidance in materials engineering. Experimentally observed scanning electron microscope (SEM) or transmission electron



microscopy (TEM) pictures are also useful to derive the morphology descriptors of nanoparticles, from which various explainable ML models such as light gradient boosted machine (LightGBM), extreme gradient boosting (XGBoost), support vector machine (SVM), and gradient boosting decision tree (GBDT) could predict the surface energy after being trained with high throughput calculations on different size scales.²¹¹

Last but not the least, the synthetic accessibility of screened candidates is an important target of material design. The synthetic accessibility is assessed to identify new efficient and synthetically accessible organic dyes for dye-sensitized solar cells (DSSCs).⁴³ The solubility and viscosity predictions are also very useful for experiments to select appropriate solvents for synthetic experiments. Feature engineering indicated that the molecular size, shape and hydrogen bonding interaction are efficient features to predict the liquid viscosity in a fast way without much loss of accuracy.²¹²

Although the well-behaved features coming from explainable ML methods could provide significant insight for experimentalists in the rational design of different kinds of materials, various deep learning methods have been introduced into chemistry and materials science. In the implementation of deep learning methods, we only need to input the information of atoms, bonds, topology, *etc.*, for each molecule. As mentioned in the above subsection, the functions of novel optical materials and electronic devices are correlated with the descriptors of dipole moment, polarizability, energy levels of the HOMO and the LUMO, and so on. In fact, the accurate prediction of the HOMO and LUMO energy levels is still a big challenge for deep learning methods. To improve the prediction accuracy of HOMO and LUMO energy levels, we proposed an efficient multi-level attention neural network, named DeepMoleNet, for molecular systems to establish an implicit relationship between the molecular structural information and 12 electronic structure properties including dipole moment, polarizability, HOMO, LUMO, HOMO–LUMO gap, zero point vibration energy (ZPVE), electronic spatial extent ($\langle R^2 \rangle$), internal energy at zero and room temperature (U_0 , U), enthalpy (H), free energy (G), and heat capacity (C_V).²¹³ In addition to these 12 quantum chemistry properties, the atom-centered symmetry functions (ACSFs)²¹⁴ descriptor is selected as the auxiliary prediction target. Recently, a modified DeepMoleNet model was proposed to study the relative stability of nanoparticles with the introduction of cut-off approximation for treating a complex system.²¹¹ It can be expected that the multi-level attention neural network is applicable to high-throughput screening of various chemical species to accelerate the rational design of material candidates.

In addition to the above-mentioned property predictions, machine learning methods have also been introduced in quantum chemical study for the prediction of atomic forces and energies, with the target of constructing accurate force fields and complicated potential energy surfaces. Shen and Yang have combined a QM/MM method and neural network (NN) for direct MD simulations.²¹⁵ The QM/MM-NN could approximately reproduce the *ab initio* QM/MM simulated results by saving the computational costs by about 2 orders of magnitude. An on-the-fly GEBF ML approach was developed to construct a machine

learning force field for oligomers by employing a Gaussian process without the need for data selection and parameter optimization.^{44,218} In this approach, only those small GEBF subsystems are employed to construct ML force fields automatically and efficiently. Then, the total energy, gradients, and molecular properties could be obtained from those of GEBF subsystems. With the GEBF-ML force field, long-time MD simulations were performed on various PE_n ($n = 20, 30, 40, 50$). The results show that the full QM energies, forces, and dipole moments of those PE could be accurately reproduced with the GEBF-ML force field. Furthermore, the infrared spectra of PE₆ obtained from the GEBF-ML MD simulations are also consistent with those from the corresponding direct AIMD or experimental results. However, the GEBF-ML MD simulations are several orders of magnitude faster than the corresponding direct GEBF-based AIMD simulations. Therefore, on-line and transfer learning force fields could be used for studying the conformation changes or vibration and even electronic spectra of long oligomers.

5 Conclusions

The development of low scaling QM methods and their combination with multiscale models and machine learning techniques has brought about fruitful applications in understanding the microscopic structure of polymeric oligomer chains, self-assembled monolayers, supramolecular complexes, and molecular aggregates in solution or solids and fast predicting various properties for speeding up material design. There are still some challenges as summarized below.

It is well known that quantum mechanics and molecular mechanics are the major tools employed in material design. Especially, DFT is widely used to compute the energy, structure, and more properties of various functional materials. However, conventional DFT calculations are still very expensive for those materials with large sizes due to their high scaling. The accuracies of DFT calculations are dependent on the choice of functionals. There are two directions to improve DFT performance for large sized systems. One blooming direction is to use ML to develop more accurate DFT functionals. The generality and transferability of trained models are crucial in this area, which requires the state-of-the-art ML models and an accurate benchmark data set for training and testing the ML derived functionals. Thus, on the other hand, high-level electron correlation methods are needed. But post HF methods are infeasible for large-sized systems and high throughput calculations because of their even higher scaling than that of DFT. For ground-state calculations, low scaling QM methods, such as fragmentation methods and local correlation methods, could speed up DFT calculations and also enable the electron correlation calculations of large systems.

We have illustrated the application of fragmentation approaches to various materials, including polymer oligomers in solutions or solids, supramolecular complexes and their molecular self-assembled, stimuli-responsive materials on surfaces and mechanically interlocked molecules. The fragmentation approaches are simple and effective, and could be



extended to various molecular or material properties with the accuracies depending on the parameters for defining local environments. However, for some complex systems such as those containing highly twined, delocalized, or polarizable functional groups, the fragments need to be manually defined. Local correlation approaches could also be employed for the calculations of relative or binding energies of supramolecular complexes. More complicated materials which are difficult to be treated by fragmentation approaches, such as metal oxides, could be computed by the local correlation methods as a black-box. Though analytic energy gradients and geometry optimization are available in the local correlation methods, high-order analytic energy derivatives are too complicated to be implemented until now. Thus, the local correlation methods have not been applied to molecular and material properties such as IR/Raman and NMR spectroscopy, which are useful characterization measurements for material systems. In addition, low scaling QM algorithms need to be improved to treat more complex systems at high QM levels. For example, two low scaling algorithms under periodic boundary conditions, such as PBC-GEBF and PBC-CIM methods, have been developed. These methods are applicable to periodic systems and need to be applied to more functional materials and interfaces. A low scaling QM dataset, such as the GEBF database⁸³ and ExL8 dataset,⁶⁴ could provide high-accuracy post HF data for both method validation and data driven molecular and material design. More low-scaling QM computation data sets with a wide range of chemical spaces are highly desired.

It has also been stressed that excited-state calculations and dynamics are important for optical functional materials such as optoelectronic devices and photo-catalysts. However, electronic excited-state calculations are much more expensive than the corresponding ground-state calculations. For the excited-state calculations, local excitation or local correlation approximation based on localized molecular orbitals or molecular fragments or excitonic models could be used to accelerate the excited-state calculations. Tensor product methods were employed to speed up the excited-state dynamics. Although the applications of low scaling excited-state methods to investigate the optoelectronic processes in organic photovoltaics have been demonstrated, the further development of quantum dynamics methodologies with an appropriate description of condensed phase environments is highly desired. The collaboration with experimental ultrafast multi-dimensional spectroscopy is also very important to provide insight into the microscopic understanding of electron-vibration coherence.

The combination of low scaling QM methods with force field based molecular dynamics simulations is still a practical way to study the packing structures of very complicated molecular aggregates in a condensed phase. The performance and transferability of the force field parameters are the key issues in material design. Electrostatics polarization could be accurately described with the assistance of the low scaling QM calculations of MD sampled configurations. However, for low-lying excited states and proton transfer reactions, much more studies are required to modify the force field forms and introduce the new idea.

So, a more general way is to apply data-mining techniques and machine learning algorithms to fast predict the energy, force, structure, and properties of functional materials. By using neural networks or other ML algorithms, the optical or electrical properties of materials could be trained from QM computational or experimental databases with some structural descriptors *via* feature learning. Then, force fields as well as material properties could be directly predicted by the trained ML models. Furthermore, the molecular energies, forces, or electronic structure properties such as HOMO and LUMO energy levels could be directly trained by ML models such as a graph convolutional NN or Gaussian process with molecular descriptors based on molecular geometries. Low scaling QM methods can be expected to accelerate the computational data generation for ML training. For example, an online transfer learning algorithm was developed for predicting the force fields, conformational structures, and IR spectra of polymer oligomers by training GEBF subsystems only.^{44,218} In the future, the online machine learning force field should also be extended to periodic materials and interfaces by taking infinite long-range electrostatic interactions into accounts. Then, the lattice energy, crystal structures, and spectroscopic properties of periodic materials could be efficiently obtained to assist the design of novel functional materials. Finally, the synthetic accessibility and theoretically designed reaction pathway could guide the experimental fabrications of materials, and in turn, the feedback from experiments could be added into the material datasets to update the ML models for the new design.

Author contributions

J. M. designed the plan and structure of the review article. W. L. and S. L. completed the review of low-scaling QM methods and their applications and ML force fields. H. M. contributed to the methods of excited states and machine learning of organic photovoltaic (OPV) materials. J. M. discussed the interplay between the experiments and simulations of stimuli-responsive monolayers and deep learning study. All authors reviewed and contributed to this manuscript.

Conflicts of interest

There are no conflicts to declare.

Acknowledgements

This work was supported by the National Natural Science Foundation of China (22033004, 21873046, 22073045, and 21833002) and the Fundamental Research Funds for the Central Universities. The authors would like to thank Ziteng Liu, Yuming Gu, Zheng Cheng, and Kang Liao for their help in collecting the data in Tables S1 and S2.†

Notes and references

- 1 S. Curtarolo, G. L. W. Hart, M. B. Nardelli, N. Mingo, S. Sanvito and O. Levy, *Nat. Mater.*, 2013, **12**, 191–201.

2 W. Y. Wang, J. Li, W. Liu and Z.-K. Liu, *Comput. Mater. Sci.*, 2019, **158**, 42–48.

3 X. Zhang, A. Chen and Z. Zhou, *Wiley Interdiscip. Rev.: Comput. Mol. Sci.*, 2019, **9**, e1385.

4 J.-L. Bredas, K. Persson and R. Seshadri, *Chem. Mater.*, 2017, **29**, 2399–2401.

5 A. Jain, Y. Shin and K. A. Persson, *Nat. Rev. Mater.*, 2016, **1**, 15004.

6 R. L. Greenaway and K. E. Jelfs, *Adv. Mater.*, 2021, **33**, 2004831.

7 K. T. Butler, J. M. Frost, J. M. Skelton, K. L. Svane and A. Walsh, *Chem. Soc. Rev.*, 2016, **45**, 6138–6146.

8 M. S. Islam and C. A. J. Fisher, *Chem. Soc. Rev.*, 2014, **43**, 185–204.

9 L. Wang, G. Nan, X. Yang, Q. Peng, Q. Li and Z. Shuai, *Chem. Soc. Rev.*, 2010, **39**, 423–434.

10 M. Muller and J. J. de Pablo, *Annu. Rev. Mater. Res.*, 2013, **43**, 1–34.

11 J. A. Elliott, *Int. Mater. Rev.*, 2011, **56**, 207–225.

12 A. H. Romero, D. C. Allan, B. Amadon, G. Antonius, T. Applencourt, L. Baguet, J. Bieder, F. Bottin, J. Bouchet, E. Bousquet, F. Bruneval, G. Brunin, D. Caliste, M. Côté, J. Denier, C. Dreyer, P. Ghosez, M. Giantomassi, Y. Gillet, O. Gingras, D. R. Hamann, G. Hautier, F. Jollet, G. Jomard, A. Martin, H. P. C. Miranda, F. Naccarato, G. Petretto, N. A. Pike, V. Planes, S. Prokhorchenko, T. Rangel, F. Ricci, G.-M. Rignanese, M. Royo, M. Stengel, M. Torrent, M. J. van Setten, B. Van Troeye, M. J. Verstraete, J. Wiktor, J. W. Zwanziger and X. Gonze, *J. Chem. Phys.*, 2020, **152**, 124102.

13 P. Verma and D. G. Truhlar, *Trends Chem.*, 2020, **2**, 302–318.

14 L. Yan, Y. Zhang, Z. Ni, Y. Zhang, J. Xu, T. Kong, J. Huang, W. Li, J. Ma and Y. Wang, *J. Am. Chem. Soc.*, 2021, **143**, 15369–15377.

15 M. Kobayashi, T. Kunisada, T. Akama, D. Sakura and H. Nakai, *J. Chem. Phys.*, 2011, **134**, 034105.

16 H. Shang, W. Liang, Y. Zhang and J. Yang, *Comput. Phys. Commun.*, 2021, **258**, 107613.

17 D. Yuan, Y. Li, W. Li and S. Li, *Phys. Chem. Chem. Phys.*, 2018, **20**, 28894–28902.

18 W. Zhang, J. Liu, X. Jin, X. Gu, X. C. Zeng, X. He and H. Li, *Angew. Chem., Int. Ed.*, 2020, **59**, 11550–11555.

19 D. S. Kaliakin, H. Nakata, Y. Kim, Q. Chen, D. G. Fedorov and L. V Slipchenko, *J. Chem. Theory Comput.*, 2020, **16**, 1175–1187.

20 H. Ma and A. Troisi, *Adv. Mater.*, 2014, **26**, 6163–6167.

21 A. F. Morrison and J. M. Herbert, *J. Phys. Chem. Lett.*, 2017, **8**, 1442–1448.

22 S. Paekel, T. Köhler, A. Swoboda, S. R. Manmana, U. Schollwöck and C. Hubig, *Ann. Phys.*, 2019, **411**, 167998.

23 H.-D. Meyer, U. Manthe and L. S. Cederbaum, *Chem. Phys. Lett.*, 1990, **165**, 73–78.

24 H. Tamura, M. Huix-Rotllant, I. Burghardt, Y. Olivier and D. Beljonne, *Phys. Rev. Lett.*, 2015, **115**, 107401.

25 F. A. Y. N. Schroder, D. H. P. Turban, A. J. Musser, N. D. M. Hine and A. W. Chin, *Nat. Commun.*, 2019, **10**, 1062.

26 X. Xie, Y. Liu, Y. Yao, U. Schollwöck, C. Liu and H. Ma, *J. Chem. Phys.*, 2019, **151**, 224101.

27 M. F. Gelin, R. Borrelli and W. Domcke, *J. Phys. Chem. Lett.*, 2019, **10**, 2806–2810.

28 S. H. M. Mehr, M. Craven, A. I. Leonov, G. Keenan and L. Cronin, *Science*, 2020, **370**, 101–108.

29 A. F. Zahrt, J. J. Henle, B. T. Rose, Y. Wang, W. T. Darrow and S. E. Denmark, *Science*, 2019, **363**, eaau5631.

30 B. Burger, P. M. Maffettone, V. V. Gusev, C. M. Aitchison, Y. Bai, X. Wang, X. Li, B. M. Alston, B. Li, R. Clowes, N. Rankin, B. Harris, R. S. Sprick and A. I. Cooper, *Nature*, 2020, **583**, 237–241.

31 B. Mikulak-Klucznik, P. Gołębiowska, A. A. Bayly, O. Popik, T. Klucznik, S. Szymkuć, E. P. Gajewska, P. Dittwald, O. Staszewska-Krajewska, W. Beker, T. Badowski, K. A. Scheidt, K. Molga, J. Mlynarski, M. Mrksich and B. A. Grzybowski, *Nature*, 2020, **588**, 83–88.

32 X. Yang, Y. Wang, R. Byrne, G. Schneider and S. Yang, *Chem. Rev.*, 2019, **119**, 10520–10594.

33 K. M. Jablonka, D. Ongari, S. M. Moosavi and B. Smit, *Chem. Rev.*, 2020, **120**, 8066–8129.

34 A. F. Zahrt, S. V Athavale and S. E. Denmark, *Chem. Rev.*, 2020, **120**, 1620–1689.

35 Y. Xu, L. Elcoro, Z.-D. Song, B. J. Wieder, M. G. Vergniory, N. Regnault, Y. Chen, C. Felser and B. A. Bernevig, *Nature*, 2020, **586**, 702–707.

36 J. G. Freeze, H. R. Kelly and V. S. Batista, *Chem. Rev.*, 2019, **119**, 6595–6612.

37 O. T. Unke, S. Chmiela, H. E. Sauceda, M. Gastegger, I. Poltavsky, K. T. Schütt, A. Tkatchenko and K.-R. Müller, *Chem. Rev.*, 2021, **121**, 10142–10186.

38 J. Westermayr and P. Marquetand, *Chem. Rev.*, 2021, **121**, 9873–9926.

39 S. Ye, K. Zhong, J. Zhang, W. Hu, J. D. Hirst, G. Zhang, S. Mukamel and J. Jiang, *J. Am. Chem. Soc.*, 2020, **142**, 19071–19077.

40 C. W. Coley, W. H. Green and K. F. Jensen, *Acc. Chem. Res.*, 2018, **51**, 1281–1289.

41 E. Cantini, X. Wang, P. Koelsch, J. A. Preece, J. Ma and P. M. Mendes, *Acc. Chem. Res.*, 2016, **49**, 1223–1231.

42 P. Liu, W. Li, Z. Kan, H. Sun and J. Ma, *J. Phys. Chem. A*, 2016, **120**, 490–502.

43 Y. Wen, L. Fu, G. Li, J. Ma and H. Ma, *Sol. RRL*, 2020, **4**, 2000110.

44 Z. Cheng, D. Zhao, J. Ma, W. Li and S. Li, *J. Phys. Chem. A*, 2020, **124**, 5007–5014.

45 S. Grimme, S. Ehrlich and L. Goerigk, *J. Comput. Chem.*, 2011, **32**, 1456–1465.

46 J.-D. Chai and M. Head-Gordon, *Phys. Chem. Chem. Phys.*, 2008, **10**, 6615.

47 M. C. Strain, G. E. Scuseria and M. J. Frisch, *Science*, 1996, **271**, 51–53.

48 S. Saebo and P. Pulay, *Annu. Rev. Phys. Chem.*, 1993, **44**, 213–236.

49 M. S. Gordon, D. G. Fedorov, S. R. Pruitt and L. V Slipchenko, *Chem. Rev.*, 2012, **112**, 632–672.



50 D. L. Strout and G. E. Scuseria, *J. Chem. Phys.*, 1995, **102**, 8448–8452.

51 E. Schwegler and M. Challacombe, *J. Chem. Phys.*, 1996, **105**, 2726–2734.

52 R. E. Stratmann, G. E. Scuseria and M. J. Frisch, *Chem. Phys. Lett.*, 1996, **257**, 213–223.

53 X. Li, J. M. Millam, G. E. Scuseria, M. J. Frisch and H. B. Schlegel, *J. Chem. Phys.*, 2003, **119**, 7651–7658.

54 S. Saebo and P. Pulay, *Chem. Phys. Lett.*, 1985, **113**, 13–18.

55 C. Hampel and H. Werner, *J. Chem. Phys.*, 1996, **104**, 6286–6297.

56 D. Usyat, L. Maschio and M. Schütz, *Wiley Interdiscip. Rev.: Comput. Mol. Sci.*, 2018, **8**, e1357.

57 M. Sparta and F. Neese, *Chem. Soc. Rev.*, 2014, **43**, 5032–5041.

58 T. Kjaergaard, P. Baudin, D. Bykov, K. Kristensen and P. Jørgensen, *Wiley Interdiscip. Rev.: Comput. Mol. Sci.*, 2017, **7**, e1319.

59 Q. Ma and H.-J. Werner, *Wiley Interdiscip. Rev.: Comput. Mol. Sci.*, 2018, **8**, e1371.

60 W. Li, Z. Ni and S. Li, *Mol. Phys.*, 2016, **114**, 1447–1460.

61 S. Li, J. Ma and Y. Jiang, *J. Comput. Chem.*, 2002, **23**, 237–244.

62 S. Li, J. Shen, W. Li and Y. Jiang, *J. Chem. Phys.*, 2006, **125**, 74109.

63 Z. Ni, Y. Wang, W. Li, P. Pulay and S. Li, *J. Chem. Theory Comput.*, 2019, **15**, 3623–3634.

64 Z. Ni, Y. Guo, F. Neese, W. Li and S. Li, *J. Chem. Theory Comput.*, 2021, **17**, 756–766.

65 W. Yang, *Phys. Rev. Lett.*, 1991, **66**, 1438–1441.

66 M. Kobayashi, T. Akama and H. Nakai, *J. Chem. Phys.*, 2006, **125**, 204106.

67 M. Kobayashi and H. Nakai, *J. Chem. Phys.*, 2009, **131**, 114108.

68 T. E. Exner and P. G. Mezey, *J. Comput. Chem.*, 2003, **24**, 1980–1986.

69 F. L. Gu, Y. Aoki, J. Korchowiec, A. Imamura and B. Kirtman, *J. Chem. Phys.*, 2004, **121**, 10385–10391.

70 X. He and J. Z. H. Zhang, *J. Chem. Phys.*, 2005, **122**, 031103.

71 W. Li and S. Li, *J. Chem. Phys.*, 2005, **122**, 194109.

72 Y. Guo, W. Li and S. Li, *Chem. Phys. Lett.*, 2012, **539–540**, 186–190.

73 M. A. Collins and R. P. A. Bettens, *Chem. Rev.*, 2015, **115**, 5607–5642.

74 J. H. Jensen, P. N. Day, M. S. Gordon, H. Basch, D. Cohen, D. R. Garmer, M. Kraus and W. J. Stevens, *Model. Hydron. Bond*, 1994, **569**, 139–151.

75 J. Gao, *J. Phys. Chem. B*, 1997, **101**, 657–663.

76 K. Kitaura, E. Ikeo, T. Asada, T. Nakano and M. Uebayasi, *Chem. Phys. Lett.*, 1999, **313**, 701–706.

77 S. Li, W. Li and T. Fang, *J. Am. Chem. Soc.*, 2005, **127**, 7215–7226.

78 V. Deev and M. A. Collins, *J. Chem. Phys.*, 2005, **122**, 154102.

79 L. Huang, L. Massa and E. Karle, *Int. J. Quantum Chem.*, 2005, **103**, 808–817.

80 N. Jiang, J. Ma and Y. Jiang, *J. Chem. Phys.*, 2006, **124**, 114112.

81 W. Li, S. Li and Y. Jiang, *J. Phys. Chem. A*, 2007, **111**, 2193–2199.

82 S. Li, W. Li and J. Ma, *Acc. Chem. Res.*, 2014, **47**, 2712–2720.

83 W. Li, H. Dong, J. Ma and S. Li, *Acc. Chem. Res.*, 2021, **54**, 169–181.

84 X. He and J. Z. H. Zhang, *J. Chem. Phys.*, 2006, **124**, 184703.

85 X. He, T. Zhu, X. Wang, J. Liu and J. Z. H. Zhang, *Acc. Chem. Res.*, 2014, **47**, 2748–2757.

86 S. R. Gadre and V. Ganesh, *J. Theor. Comput. Chem.*, 2006, **05**, 835–855.

87 N. J. Mayhall and K. Raghavachari, *J. Chem. Theory Comput.*, 2011, **7**, 1336–1343.

88 R. M. Richard and J. M. Herbert, *J. Chem. Phys.*, 2012, **137**, 064113.

89 K. Raghavachari and A. Saha, *Chem. Rev.*, 2015, **115**, 5643–5677.

90 J. M. Herbert, *J. Chem. Phys.*, 2019, **151**, 170901.

91 H. Stoll, *Chem. Phys. Lett.*, 1992, **191**, 548–552.

92 C. Pisani, M. Busso, G. Capecchi, S. Casassa, R. Dovesi, L. Maschio, C. Zicovich-Wilson and M. Schütz, *J. Chem. Phys.*, 2005, **122**, 094113.

93 E. Rebolini, G. Baardsen, A. S. Hansen, K. R. Leikanger and T. B. Pedersen, *J. Chem. Theory Comput.*, 2018, **14**, 2427–2438.

94 Y. Wang, Z. Ni, W. Li and S. Li, *J. Chem. Theory Comput.*, 2019, **15**, 2933–2943.

95 J. Yang, W. Hu, D. Usyat, D. Matthews, M. Schütz and G. K.-L. Chan, *Science*, 2014, **345**, 640–643.

96 T. Fang, W. Li, F. Gu and S. Li, *J. Chem. Theory Comput.*, 2015, **11**, 91–98.

97 T. Fang, Y. Li and S. Li, *Wiley Interdiscip. Rev.: Comput. Mol. Sci.*, 2017, **7**, e1297.

98 M. J. S. Dewar, E. G. Zoebisch, E. F. Healy and J. J. P. Stewart, *J. Am. Chem. Soc.*, 1985, **107**, 3902–3909.

99 J. J. P. Stewart, *J. Mol. Model.*, 2007, **13**, 1173–1213.

100 M. Elstner, D. Porezag, G. Jungnickel, J. Elsner, M. Haugk, T. Frauenheim, S. Suhai and G. Seifert, *Phys. Rev. B: Condens. Matter Mater. Phys.*, 1998, **58**, 7260–7268.

101 G. Seifert and J.-O. Joswig, *Wiley Interdiscip. Rev.: Comput. Mol. Sci.*, 2012, **2**, 456–465.

102 C. Bannwarth, E. Caldeweyher, S. Ehlert, A. Hansen, P. Pracht, J. Seibert, S. Spicher and S. Grimme, *Wiley Interdiscip. Rev.: Comput. Mol. Sci.*, 2021, **11**, e1493.

103 Y. Nishimoto, D. G. Fedorov and S. Irle, *Chem. Phys. Lett.*, 2015, **636**, 90–96.

104 H. Nishizawa, Y. Nishimura, M. Kobayashi, S. Irle and H. Nakai, *J. Comput. Chem.*, 2016, **37**, 1983–1992.

105 D. Mester and M. Kállay, *J. Chem. Theory Comput.*, 2019, **15**, 1690–1704.

106 M. Miura and Y. Aoki, *J. Comput. Chem.*, 2009, **30**, 2213–2230.

107 R. A. Mata and H. Stoll, *J. Chem. Phys.*, 2011, **134**, 034122.

108 C. Zhang, D. Yuan, Y. Guo and S. Li, *J. Chem. Theory Comput.*, 2014, **10**, 5308–5317.

109 J. Liu and J. M. Herbert, *J. Chem. Theory Comput.*, 2016, **12**, 157–166.



110 X. Jin, W. J. Glover and X. He, *J. Chem. Theory Comput.*, 2020, **16**, 5174–5188.

111 W. Li, Y. Li, R. Lin and S. Li, *J. Phys. Chem. A*, 2016, **120**, 9667–9677.

112 G. Macetti and A. Genoni, *J. Chem. Theory Comput.*, 2020, **16**, 7490–7506.

113 W.-K. Chen, W.-H. Fang and G. Cui, *J. Phys. Chem. Lett.*, 2019, **10**, 7836–7841.

114 C. Yam, S. Yokojima and G. Chen, *Phys. Rev. B: Condens. Matter Mater. Phys.*, 2003, **68**, 153105.

115 G. Cui, W. Fang and W. Yang, *Phys. Chem. Chem. Phys.*, 2010, **12**, 416–421.

116 F. Wu, W. Liu, Y. Zhang and Z. Li, *J. Chem. Theory Comput.*, 2011, **7**, 3643–3660.

117 T. D. Crawford and R. A. King, *Chem. Phys. Lett.*, 2002, **366**, 611–622.

118 D. Kats, T. Korona and M. Schütz, *J. Chem. Phys.*, 2006, **125**, 104106.

119 T. S. Chwee and E. A. Carter, *J. Chem. Theory Comput.*, 2011, **7**, 103–111.

120 Q. Li, Q. Li and Z. Shuai, *Synth. Met.*, 2008, **158**, 330–335.

121 H. Nakatsuji, T. Miyahara and R. Fukuda, *J. Chem. Phys.*, 2007, **126**, 084104.

122 H. Nakai and T. Yoshikawa, *J. Chem. Phys.*, 2017, **146**, 124123.

123 T. Yoshikawa, J. Yoshihara and H. Nakai, *J. Chem. Phys.*, 2020, **152**, 024102.

124 S. Nishio and Y. Kurashige, *J. Chem. Phys.*, 2019, **151**, 084110.

125 S.-H. Lim, T. G. Bjorklund, F. C. Spano and C. J. Bardeen, *Phys. Rev. Lett.*, 2004, **92**, 107402.

126 N. J. Hestand, R. V. Kazantsev, A. S. Weingarten, L. C. Palmer, S. I. Stupp and F. C. Spano, *J. Am. Chem. Soc.*, 2016, **138**, 11762–11774.

127 X. Li, R. M. Parrish, F. Liu, S. I. L. Kokkila Schumacher and T. J. Martínez, *J. Chem. Theory Comput.*, 2017, **13**, 3493–3504.

128 J. Wen and H. Ma, *Chem. Phys. Lett.*, 2017, **679**, 152–157.

129 H. Zhao, Y. Zhao, Y. Song, M. Zhou, W. Lv, L. Tao, Y. Feng, B. Song, Y. Ma, J. Zhang, J. Xiao, Y. Wang, D.-H. Lien, M. Amani, H. Kim, X. Chen, Z. Wu, Z. Ni, P. Wang, Y. Shi, H. Ma, X. Zhang, J.-B. Xu, A. Troisi, A. Javey and X. Wang, *Nat. Commun.*, 2019, **10**, 5589.

130 J. A. Green, H. Asha, F. Santoro and R. Improta, *J. Chem. Theory Comput.*, 2021, **17**, 405–415.

131 T. Fujita and Y. Mochizuki, *J. Phys. Chem. A*, 2018, **122**, 3886–3898.

132 C. Bloch, *Nucl. Phys.*, 1958, **6**, 329–347.

133 C. J. Morningstar and M. Weinstein, *Phys. Rev. Lett.*, 1994, **73**, 1873–1877.

134 M. Al Hajj, J.-P. Malrieu and N. Guihéry, *Phys. Rev. B*, 2005, **72**, 224412.

135 H. Zhang, J. P. Malrieu, H. Ma and J. Ma, *J. Comput. Chem.*, 2012, **33**, 34–43.

136 Y. Ma, Y. Liu and H. Ma, *J. Chem. Phys.*, 2012, **136**, 024113.

137 Y. Ma and H. Ma, *J. Phys. Chem. A*, 2013, **117**, 3655–3665.

138 T. G. Kolda and B. W. Bader, *SIAM Rev.*, 2009, **51**, 455–500.

139 L. R. Tucker, *Psychometrika*, 1966, **31**, 279–311.

140 L. De Lathauwer, B. De Moor and J. Vandewalle, *SIAM J. Matrix Anal. Appl.*, 2000, **21**, 1253–1278.

141 H. Wang and M. Thoss, *J. Chem. Phys.*, 2003, **119**, 1289–1299.

142 I. V. Oseledets, *SIAM J. Sci. Comput.*, 2011, **33**, 2295–2317.

143 F. Verstraete, V. Murg and J. I. Cirac, *Adv. Phys.*, 2008, **57**, 143–224.

144 S. R. White, *Phys. Rev. Lett.*, 1992, **69**, 2863–2866.

145 U. Schollwock, *Rev. Mod. Phys.*, 2005, **77**, 259–315.

146 Y. Yao, K.-W. Sun, Z. Luo and H. Ma, *J. Phys. Chem. Lett.*, 2018, **9**, 413–419.

147 H. Ma, Z. Luo and Y. Yao, *Mol. Phys.*, 2018, **116**, 854–868.

148 J. Ren, Z. Shuai and G. Kin-Lic Chan, *J. Chem. Theory Comput.*, 2018, **14**, 5027–5039.

149 W. Popp, M. Polkehn, R. Binder and I. Burghardt, *J. Phys. Chem. Lett.*, 2019, **10**, 3326–3332.

150 A. Baiardi and M. Reiher, *J. Chem. Theory Comput.*, 2019, **15**, 3481–3498.

151 W. Li, J. Ren and Z. Shuai, *J. Phys. Chem. Lett.*, 2020, **11**, 4930–4936.

152 J. Zheng, J. Peng, Y. Xie, Y. Long, X. Ning and Z. Lan, *Phys. Chem. Chem. Phys.*, 2020, **22**, 18192–18204.

153 T. A. Niehaus, D. Heringer, B. Torralva and T. Frauenheim, *Eur. Phys. J. D*, 2005, **35**, 467–477.

154 S. Grimme and C. Bannwarth, *J. Chem. Phys.*, 2016, **145**, 054103.

155 M. Inamori, T. Yoshikawa, Y. Ikabata, Y. Nishimura and H. Nakai, *J. Comput. Chem.*, 2020, **41**, 1538–1548.

156 T. Yoshikawa, N. Komoto, Y. Nishimura and H. Nakai, *J. Comput. Chem.*, 2019, **40**, 2778–2786.

157 W. Li, M. Duan, K. Liao, B. Hong, Z. Ni, J. Ma and S. Li, *Electron. Struct.*, 2019, **1**, 044003.

158 Y. Guo, W. Li and S. Li, *J. Phys. Chem. A*, 2014, **118**, 8996–9004.

159 Y. Guo, U. Becker and F. Neese, *J. Chem. Phys.*, 2018, **148**, 124117.

160 J. C. A. Prentice, J. Aarons, J. C. Womack, A. E. A. Allen, L. Andrinopoulos, L. Anton, R. A. Bell, A. Bhandari, G. A. Bramley, R. J. Charlton, R. J. Clements, D. J. Cole, G. Constantinescu, F. Corsetti, S. M.-M. Dubois, K. K. B. Duff, J. M. Escartín, A. Greco, Q. Hill, L. P. Lee, E. Linscott, D. D. O'Regan, M. J. S. Phipps, L. E. Ratcliff, Á. R. Serrano, E. W. Tait, G. Teobaldi, V. Vitale, N. Yeung, T. J. Zuehlsdorff, J. Dziedzic, P. D. Haynes, N. D. M. Hine, A. A. Mostofi, M. C. Payne and C.-K. Skylaris, *J. Chem. Phys.*, 2020, **152**, 174111.

161 X. Qin, H. Shang, H. Xiang, Z. Li and J. Yang, *Int. J. Quantum Chem.*, 2015, **115**, 647–655.

162 W. Li, C. Chen, D. Zhao and S. Li, *Int. J. Quantum Chem.*, 2015, **115**, 641–646.

163 G. M. J. Barca, C. Bertoni, L. Carrington, D. Datta, N. De Silva, J. E. Deustua, D. G. Fedorov, J. R. Gour, A. O. Gunina, E. Guidez, T. Harville, S. Irle, J. Ivanic, K. Kowalski, S. S. Leang, H. Li, W. Li, J. J. Lutz, I. Magoulas, J. Mato, V. Mironov, H. Nakata, B. Q. Pham, P. Piecuch, D. Poole, S. R. Pruitt, A. P. Rendell,



L. B. Roskop, K. Ruedenberg, T. Sattasathuchana, M. W. Schmidt, J. Shen, L. Slipchenko, M. Sosonkina, V. Sundriyal, A. Tiwari, J. L. Galvez Vallejo, B. Westheimer, M. Włoch, P. Xu, F. Zahariev and M. S. Gordon, *J. Chem. Phys.*, 2020, **152**, 154102.

164 H.-J. Werner, P. J. Knowles, F. R. Manby, J. A. Black, K. Doll, A. Heßelmann, D. Kats, A. Köhn, T. Korona, D. A. Kreplin, Q. Ma, T. F. Miller, A. Mitrushchenkov, K. A. Peterson, I. Polyak, G. Rauhut and M. Sibaev, *J. Chem. Phys.*, 2020, **152**, 144107.

165 F. Neese, F. Wennmohs, U. Becker and C. Riplinger, *J. Chem. Phys.*, 2020, **152**, 224108.

166 R. Dovesi, F. Pascale, B. Civalleri, K. Doll, N. M. Harrison, I. Bush, P. D'Arco, Y. Noël, M. Rérat, P. Carbonnière, M. Causà, S. Salustro, V. Lacivita, B. Kirtman, A. M. Ferrari, F. S. Gentile, J. Baima, M. Ferrero, R. Demichelis and M. De La Pierre, *J. Chem. Phys.*, 2020, **152**, 204111.

167 T. D. Kühne, M. Iannuzzi, M. Del Ben, V. V Rybkin, P. Seewald, F. Stein, T. Laino, R. Z. Khalilullin, O. Schütt, F. Schiffmann, D. Golze, J. Wilhelm, S. Chulkov, M. H. Bani-Hashemian, V. Weber, U. Borštník, M. Taillefumier, A. S. Jakobovits, A. Lazzaro, H. Pabst, T. Müller, R. Schade, M. Guidon, S. Andermatt, N. Holmberg, G. K. Schenter, A. Hehn, A. Bussy, F. Belleflamme, G. Tabacchi, A. Glöß, M. Lass, I. Bethune, C. J. Mundy, C. Plessl, M. Watkins, J. VandeVondele, M. Krack and J. Hutter, *J. Chem. Phys.*, 2020, **152**, 194103.

168 B. Hourahine, B. Aradi, V. Blum, F. Bonafé, A. Buccheri, C. Camacho, C. Cevallos, M. Y. Deshaye, T. Dumitrică, A. Dominguez, S. Ehlert, M. Elstner, T. van der Heide, J. Hermann, S. Irle, J. J. Kranz, C. Köhler, T. Kowalczyk, T. Kubář, I. S. Lee, V. Lutsker, R. J. Maurer, S. K. Min, I. Mitchell, C. Negre, T. A. Niehaus, A. M. N. Niklasson, A. J. Page, A. Pecchia, G. Penazzi, M. P. Persson, J. Řezáč, C. G. Sánchez, M. Sternberg, M. Stöhr, F. Stuckenberg, A. Tkatchenko, V. W.-z. Yu and T. Frauenheim, *J. Chem. Phys.*, 2020, **152**, 124101.

169 W. Hu, L. Lin, C. Yang and J. Yang, *J. Chem. Phys.*, 2014, **141**, 214704.

170 Z. Luo, X. Qin, L. Wan, W. Hu and J. Yang, *Front. Chem.*, 2020, **8**, 932.

171 H. Li, W. Li, S. Li and J. Ma, *J. Phys. Chem. B*, 2008, **112**, 7061–7070.

172 H. Cao, T. Fang, S. Li and J. Ma, *Macromolecules*, 2007, **40**, 4363–4369.

173 X. Yuan, W. Zhang, L. H. Xie, J. Ma, W. Huang and W. Liu, *J. Phys. Chem. B*, 2015, **119**, 10316–10333.

174 S. Hua, W. Hua and S. Li, *J. Phys. Chem. A*, 2010, **114**, 8126–8134.

175 W. Liang, S. Yokojima and G. Chen, *J. Chem. Phys.*, 2000, **113**, 1403–1408.

176 M. Kobayashi and H. Nakai, *Phys. Chem. Chem. Phys.*, 2012, **14**, 7629.

177 G. Boschetto, H.-T. Xue, J. Dziedzic, M. Krompiec and C.-K. Skylaris, *J. Phys. Chem. C*, 2017, **121**, 2529–2538.

178 S. Chen and J. Ma, *J. Chem. Phys.*, 2012, **137**, 074708.

179 J. Wen and J. Ma, *J. Phys. Chem. C*, 2012, **116**, 8523–8534.

180 R. Sure and S. Grimme, *J. Chem. Theory Comput.*, 2015, **11**, 3785–3801.

181 K. Liao, S. Wang, W. Li and S. Li, *Phys. Chem. Chem. Phys.*, 2021, **23**, 19394–19401.

182 T. Schaller, U. P. Büchele, F.-G. Klärner, D. Bläser, R. Boese, S. P. Brown, H. W. Spiess, F. Koziol, J. Kussmann and C. Ochsenfeld, *J. Am. Chem. Soc.*, 2007, **129**, 1293–1303.

183 N. Jiang, R. X. Tan and J. Ma, *J. Phys. Chem. B*, 2011, **115**, 2801–2813.

184 Y. Chen, L. Fu, B. Sun, C. Qian, R. Wang, J. Jiang, C. Lin, J. Ma and L. Wang, *Org. Lett.*, 2020, **22**, 2266–2270.

185 T. Kjaergaard, P. Baudin, D. Bykov, J. J. Eriksen, P. Ettenhuber, K. Kristensen, J. Larkin, D. Liakh, F. Pawłowski, A. Vose, Y. M. Wang and P. Jorgensen, *Comput. Phys. Commun.*, 2017, **212**, 152–160.

186 S. Debnath, A. Sengupta, K. V. J. Jose and K. Raghavachari, *J. Chem. Theory Comput.*, 2018, **14**, 6226–6239.

187 J. Lahann, S. Mitragotri, T.-N. Tran, H. Kaido, J. Sundaram, I. S. Choi, S. Hoffer, G. A. Somorjai and R. Langer, *Science*, 2003, **299**, 371–374.

188 J. Zhao, X. Wang, N. Jiang, T. Yan, Z. Kan, P. M. Mendes and J. Ma, *J. Phys. Chem. C*, 2015, **119**, 22866–22881.

189 C. L. Yeung, X. Wang, M. Lashkar, E. Cantini, F. J. Rawson, P. Iqbal, J. A. Preece, J. Ma and P. M. Mendes, *Adv. Mater. Interfaces*, 2014, **1**, 1300085.

190 J. Wen, Z. Tian and J. Ma, *J. Phys. Chem. C*, 2013, **117**, 19934–19944.

191 Y. Pei and J. Ma, *J. Am. Chem. Soc.*, 2005, **127**, 6802–6813.

192 A. N. Brigeman, M. A. Fusella, Y. Yan, G. E. Purdum, Y.-L. Loo, B. P. Rand and N. C. Giebink, *Adv. Energy Mater.*, 2016, **6**, 1601001.

193 S. Sharma, K. Sivalingam, F. Neese and G. K.-L. Chan, *Nat. Chem.*, 2014, **6**, 927–933.

194 B. E. Van Kuiken, A. W. Hahn, B. Nayyar, C. E. Schiewer, S. C. Lee, F. Meyer, T. Weyhermüller, A. Nicolaou, Y.-T. Cui, J. Miyawaki, Y. Harada and S. DeBeer, *Inorg. Chem.*, 2018, **57**, 7355–7361.

195 D. Cho, J. R. Rouxel, S. Mukamel, G. Kin-Lic Chan and Z. Li, *J. Phys. Chem. Lett.*, 2019, **10**, 6664–6671.

196 M. F. Gelin and R. Borrelli, *J. Chem. Theory Comput.*, 2021, **17**, 4316–4331.

197 D. Casanova, *Chem. Rev.*, 2018, **118**, 7164–7207.

198 Z. Wang, H. Liu, X. Xie, C. Zhang, R. Wang, L. Chen, Y. Xu, H. Ma, W. Fang, Y. Yao, H. Sang, X. Wang, X. Li and M. Xiao, *Nat. Chem.*, 2021, **13**, 559–567.

199 S. Mardazad, Y. Xu, X. Yang, M. Grundner, U. Schollwöck, H. Ma and S. Paeckel, 2021, arXiv: 2107.13948.

200 W. Li, J. Ren and Z. Shuai, *Nat. Commun.*, 2021, **12**, 4260.

201 B. Kailkhura, B. Gallagher, S. Kim, A. Hiszpanski and T. Y.-J. Han, *npj Comput. Mater.*, 2019, **5**, 108.

202 S. A. Lopez, B. Sanchez-Lengeling, J. de Goes Soares and A. Aspuru-Guzik, *Joule*, 2017, **1**, 857–870.

203 D. Padula, J. D. Simpson and A. Troisi, *Mater. Horiz.*, 2019, **6**, 343–349.

204 D. Padula and A. Troisi, *Adv. Energy Mater.*, 2019, **9**, 1902463.



205 W. Sun, Y. Zheng, K. Yang, Q. Zhang, A. A. Shah, Z. Wu, Y. Sun, L. Feng, D. Chen, Z. Xiao, S. Lu, Y. Li and K. Sun, *Sci. Adv.*, 2019, **5**, eaay4275.

206 S.-P. Peng and Y. Zhao, *J. Chem. Inf. Model.*, 2019, **59**, 4993–5001.

207 H. Sahu, W. Rao, A. Troisi and H. Ma, *Adv. Energy Mater.*, 2018, **8**, 1801032.

208 H. Sahu and H. Ma, *J. Phys. Chem. Lett.*, 2019, **10**, 7277–7284.

209 H. Sahu, F. Yang, X. Ye, J. Ma, W. Fang and H. Ma, *J. Mater. Chem. A*, 2019, **7**, 17480–17488.

210 Y. Wen, Y. Liu, B. Yan, T. Gaudin, J. Ma and H. Ma, *J. Phys. Chem. Lett.*, 2021, **12**, 4980–4986.

211 Z. Liu, Y. Shi, H. Chen, T. Qin, X. Zhou, J. Huo, H. Dong, X. Yang, X. Zhu, X. Chen, L. Zhang, M. Yang, Y. Gao and J. Ma, *npj Comput. Mater.*, 2021, **7**, 142.

212 Q. Zhu, Y. Gu, L. Hu, T. Gaudin, M. Fan and J. Ma, *J. Chem. Phys.*, 2021, **154**, 74502.

213 Z. Liu, L. Lin, Q. Jia, Z. Cheng, Y. Jiang, Y. Guo and J. Ma, *J. Chem. Inf. Model.*, 2021, **61**, 1066–1082.

214 J. Behler, *J. Chem. Phys.*, 2011, **134**, 074106.

215 L. Shen and W. Yang, *J. Chem. Theory Comput.*, 2018, **14**, 1442–1455.

216 H. M. Netzloff and M. A. Collins, *J. Chem. Phys.*, 2007, **127**(13), 134113.

217 G. J. O. Beran and K. Nanda, *J. Phys. Chem. Lett.*, 2010, **1**(24), 3480–3487.

218 Z. Cheng, J. Du, L. Zhang, J. Ma, W. Li and S. Li, *Phys. Chem. Chem. Phys.*, 2021, DOI: 10.1039/D1CP03934B.

